

A structure-preserving LDG discretization of the Fisher-Kolmogorov equation for modeling neurodegenerative diseases

Paola F. Antonietti * Mattia Corti * Sergio Gómez † Ilaria Perugia ‡

Abstract

This work presents a structure-preserving, high-order, unconditionally stable numerical method for approximating the solution to the Fisher-Kolmogorov equation on polytopal meshes, with a particular focus on its application in simulating misfolded protein spreading in neurodegenerative diseases. The model problem is reformulated using an entropy variable to guarantee solution positivity, boundedness, and satisfaction of a discrete entropy-stability inequality at the numerical level. The scheme combines a local discontinuous Galerkin method on polytopal meshes for the space discretization with a ν -step backward differentiation formula for the time integration. Implementation details are discussed, including a detailed derivation of the linear systems arising from Newton’s iteration. The accuracy and robustness of the proposed method are demonstrated through extensive numerical tests. Finally, the method’s practical performance is demonstrated through simulations of α -synuclein propagation in a two-dimensional brain geometry segmented from MRI data, providing a relevant computational framework for modeling synucleopathies (such as Parkinson’s disease) and, more generally, neurodegenerative diseases.

Keywords. Fisher-Kolmogorov equation, structure-preserving discretizations, local discontinuous Galerkin method, polytopal meshes, modeling of neurodegenerative diseases.

Mathematics Subject Classification. 65M60, 65N22, 35Q92

1 Introduction

The Fisher-Kolmogorov (FK) equation, also known as the Fisher-Kolmogorov-Petrovsky-Piskunov (Fisher-KPP) equation, is a reaction-diffusion equation that models the dynamics of biological populations or advantageous genes [1]. The FK equation combines a diffusion term with a non-linear reaction component, accounting for growth and saturation effects. In recent years, its application has become increasingly prominent in modeling neurodegenerative diseases, particularly within the framework of the *prion-like* hypothesis [2]. This hypothesis suggests that misfolded proteins, such as α -synuclein in Parkinson’s disease or dementia with Lewy Bodies (DLB) [3], and amyloid- β and tau in the context of Alzheimer’s disease [4], propagate throughout the brain like infectious agents, transitioning from one region to another. Consequently, the FK equation provides a valuable mathematical framework capable of addressing misfolded proteins dynamics, local proliferation dynamics, and their spread through brain networks. At the continuous level, the key variables—population density or pathological protein concentration—are inherently nonnegative and constrained by physical and biological limits. Indeed, from a mathematical viewpoint, it can be proved that the solution to the FK equation with homogeneous Neumann boundary conditions remains nonnegative and bounded as long as the initial conditions are nonnegative and the reaction term satisfies appropriate biological constraints corresponding to the absence and saturation of the population or pathological agent, respectively [5]. When moving from the infinite-dimensional setting to the discrete one, it is crucial to develop numerical discretization methods that preserve the nonnegativity and boundedness of the discrete solution. Additionally, they should reproduce key structural properties of the continuous problem to ensure consistency with the underlying model. Such schemes are referred to as *structure-preserving* (encompassing positivity- and bound-preservation).

*MOX-Dipartimento di Matematica, Politecnico di Milano, Piazza Leonardo da Vinci 32, Milan, 20133, Italy (paola.antonietti@polimi.it, mattia.corti@polimi.it)

†Department of Mathematics and Applications, University of Milano-Bicocca, Via Cozzi 55, Milan, 20125, Italy (sergio.gomezmacias@unimib.it)

‡Faculty of Mathematics, University of Vienna, Oskar-Morgenstern-Platz 1, 1090 Vienna, Austria (ilaria.perugia@univie.ac.at)

Discontinuous Galerkin (DG) methods have been effectively employed to discretize FK equations owing to their flexibility in handling complex and heterogeneous computational domains, as well as their ability to accommodate (element-wise) high-order approximations, which is pivotal for accurately capturing traveling-wave solutions. These features are particularly significant in the modeling of neurodegenerative diseases, where the underlying geometry is complex, with intricate details and highly heterogeneous media, and where phenomena occur at long time scales. DG schemes were first introduced in the early seventies for first-order hyperbolic problems, as referenced in [6]. The development of DG schemes for second-order elliptic problems can be traced back to [7] and [8–11]; see also [12]. To further enhance geometric flexibility, DG methods on polytopal grids (PolyDG) have been proposed for the numerical discretization of a broad range of differential problems, see e.g., [13–16], the references therein, the comprehensive monograph [17], and the review [18]. PolyDG discretizations of FK equations have been studied in [19] and have been extended to encompass more physics-informed models in neurodegeneration, including the heterodimer model [20,21]. Nonetheless, numerical discretizations written in the primal variable, i.e. the pathological protein concentration for our application of interest, are not inherently structure-preserving. In some cases, they may produce discrete solutions with nonphysical negative values or values that exceed biologically plausible limits. This can occur, for example, when approximating steep gradients or using coarse meshes.

The design of structure-preserving DG methods is a well-established area of research. Positivity-preserving DG schemes for parabolic equations have been developed, e.g., in [22–24]. For the FK equation, positivity-preserving schemes have been explored in the context of finite-difference approximations (see, e.g., [25,26]) and of continuous finite-element discretizations (see, e.g., [27]). A possible approach to devise a positivity-preserving scheme for the FK equation involves rewriting the original model by changing variables. Instead of solving for the original field, the system is reformulated in terms of an entropy variable. In this context, an entropy-stable, structure-preserving DG scheme on simplicial grids for the FK equation has been proposed and analyzed in [28] and further extended to polytopal grids in [19]. The latter work also provided a thorough validation in the context of modeling the accumulation and spread of prionic proteins, showing accurate solutions for biologically meaningful, stable, and accurate simulations of disease progression. In [29], a structure-preserving local discontinuous Galerkin (LDG) method on simplicial grids for non-linear cross-diffusion systems that exploits the boundedness-by-entropy framework of [30] is presented and analyzed. In the context of linear diffusion, the variable transformation utilized in [28], see also [19], introduces a non-linearity in the diffusion tensor, complicating the practical implementation of the discrete problem. First, the penalty function in the DG discretization of the diffusion term depends on the new auxiliary variable obtained from the exponential transformation and necessitates careful calibration. Furthermore, due to the fact that non-linearities appear in the differential operator, Newton’s iterations may exhibit poor conditioning, especially when approximation spaces with large polynomial degrees are employed.

This paper aims to specialize the approach proposed in [29] to the FK equation. The main idea is to exploit the underlying entropy structure of the problem and first rewrite it in appropriately chosen auxiliary variables in such a way that the non-linearities do not occur within differential operators or interface terms, but only in zero-order terms. At the same time, such a transformation allows the physical positivity and boundedness to be satisfied in a strong sense. Next, an LDG method on polytopal grids for the space discretization, combined with a ν -step backward differentiation formula (BDF) for the time discretization, is employed for the numerical approximation. The resulting method inherently preserves positivity and boundedness of solutions and, at least in the case of BDF1 (backward Euler), satisfies an entropy stability inequality similar to that of the original problem. Additionally, since non-linearities arise only in volume terms, these can be computed massively in parallel element-by-element, exploiting the fact that volume terms are block diagonal in the DG framework. As a result, we achieve improved stability of the scheme and avoid the need for fine-tuning stability parameters.

The remaining part of the manuscript is structured as follows. In Section 2, we introduce the model problem, reformulate it using a suitable entropy variable, and present its structure-preserving LDG space discretization on polytopal grids, coupled with a ν -step BDF time integration scheme. Section 2 also discusses implementation details, including an explicit derivation of the linear systems stemming from Newton’s iteration. Section 3 provides an extensive numerical verification of the accuracy of the proposed structure-preserving BDF-LDG method through test cases with known analytical solutions. Finally, Section 4 presents computations aimed at demonstrating the practical performance of the proposed method in modeling α -synuclein protein spreading, which is involved in relevant neurodegenerative diseases such as Parkinson’s disease, dementia with Lewy bodies, and Alzheimer’s disease with Lewy bodies. The results in this section have been obtained on a two-dimensional section of a brain geometry, segmented from a structural magnetic resonance image.

2 Model problem and numerical discretization

Let $\Omega \subset \mathbb{R}^d$ ($d \in \{2, 3\}$) be a polytopical space domain with Lipschitz boundary $\Gamma := \partial\Omega$ and outward-pointing normal unit vector \mathbf{n}_Ω , and let $(0, T)$ be a time interval, with $T > 0$. In the space-time cylinder $Q_T := \Omega \times (0, T)$, we consider the following initial and boundary value problem for the Fisher-Kolmogorov (FK) equation: find $c : Q_T \rightarrow \mathbb{R}$ such that

$$\partial_t c - \nabla \cdot (\mathbf{D} \nabla c) = \alpha c(1 - c) =: f(c) \quad \text{in } Q_T, \quad (2.1a)$$

$$(\mathbf{D} \nabla c) \cdot \mathbf{n}_\Omega = \mathbf{0} \quad \text{on } \Gamma \times (0, T), \quad (2.1b)$$

$$c(\cdot, 0) = c_0 \quad \text{in } \Omega. \quad (2.1c)$$

Here, the coefficient $\alpha = \alpha(\mathbf{x}) \in L^\infty(\Omega)$ is strictly positive, and the diffusion tensor $\mathbf{D} = \mathbf{D}(\mathbf{x}) \in L^\infty(\Omega)^{d \times d}$ is assumed to be symmetric and uniformly positive definite, namely there exists a constant $D_0 > 0$ such that

$$\mathbf{z}^\top \mathbf{D} \mathbf{z} \geq D_0 |\mathbf{z}|^2 \quad \forall \mathbf{z} \in \mathbb{R}^d. \quad (2.2)$$

Additionally, we assume that $0 \leq c_0 \leq 1$ a.e. in Ω , so that

$$0 \leq c(\mathbf{x}, t) \leq 1 \quad \text{for almost all } (\mathbf{x}, t) \in Q_T; \quad (2.3)$$

see [5, §2.10.2].

Next, we introduce our structure-preserving LDG method. We start by reformulating the problem in an entropy variable in Section 2.1, then we define the method in Section 2.2, and write it in matrix form in Section 2.3. Henceforth, given a domain \mathcal{D} , we use $(\cdot, \cdot)_{\mathcal{D}}$ to denote the $L^2(\mathcal{D})$ inner product, and $|\mathcal{D}|$ its measure.

2.1 Reformulation in terms of an entropy variable

The change of variable

$$c = u(w) := \frac{e^w}{1 + e^w}, \quad w : Q_T \rightarrow \mathbb{R}, \quad (2.4)$$

enforces that c satisfies the bound in (2.3). In the setting of [29, 30], this corresponds to writing $u = (s')^{-1}$, with the *entropy function* s defined by

$$s(c) := c \log c + (1 - c) \log(1 - c) \geq 0,$$

for which

$$s'(c) = \log c - \log(1 - c) = \log\left(\frac{c}{1 - c}\right), \quad s''(c) = \frac{1}{c(1 - c)}.$$

Such an entropy function satisfies the following properties:

$$s''(c) \geq 4 \quad \forall c \in (0, 1), \quad (2.5a)$$

$$|\alpha(\mathbf{x})c(1 - c)s'(c)| \leq C_f \|\alpha\|_{L^\infty(\Omega)} \quad \text{for a.e. } \mathbf{x} \in \Omega, \quad \forall c \in (0, 1), \quad (2.5b)$$

with $C_f = \max_{c \in [0, 1]} |c(1 - c)s'(c)| \leq 0.25$. As $w = s'(c)$, the chain rule gives

$$\nabla w = s''(c) \nabla c. \quad (2.6)$$

We introduce the following auxiliary variables in Q_T :

$$w \text{ s.t. } c = u(w), \quad (2.7a)$$

$$\mathbf{z} := -\nabla w, \quad (2.7b)$$

$$\mathbf{D} s''(c) \boldsymbol{\sigma} := -\mathbf{D} s''(c) \nabla c = \mathbf{D} \mathbf{z}, \quad (2.7c)$$

$$\mathbf{r} := \mathbf{D} \boldsymbol{\sigma}. \quad (2.7d)$$

The first identity in equation (2.7c) imposes $\boldsymbol{\sigma} = -\nabla c$, due to the invertibility of \mathbf{D} and the fact that s'' is bounded away from zero. More precisely, $s''(c)\mathbf{D}$ is uniformly positive definite with constant $4D_0$, where D_0 is the constant in (2.2):

$$\mathbf{z}^\top (s''(c)\mathbf{D}) \mathbf{z} \geq \left(\inf_{(\mathbf{x}, t) \in Q_T} s''(c(\mathbf{x}, t)) \right) D_0 |\mathbf{z}|^2 \geq 4D_0 |\mathbf{z}|^2 \quad \forall \mathbf{z} \in \mathbb{R}^d. \quad (2.8)$$

After applying the change of variables in equation (2.7a), the definition of the auxiliary variables follows the standard LDG approach, avoiding the presence of non-linearities under differential operators. This is achieved by imposing the chain rule in equation (2.6). Specifically, we define $\mathbf{r} := -\mathbf{D}\nabla c$ (equation (2.7d)), writing $\boldsymbol{\sigma} = -\nabla c$ (first identity in (2.7c)). The second identity in (2.7c), along with equation (2.7b), enforces the chain rule in equation (2.6), avoiding that $\nabla c = \nabla(u(w))$ appears in the formulation. The variable \mathbf{r} then represent the flux of c and will appear explicitly in the formulation (see (2.9) below).

Problem (2.1) is reformulated in the variables defined in (2.7) as follows: find $w : Q_T \rightarrow \mathbb{R}$ and $\mathbf{r} : Q_T \rightarrow \mathbb{R}^d$ such that

$$\partial_t c + \nabla \cdot \mathbf{r} = \alpha c(1 - c) = f(c) \quad \text{in } Q_T, \quad (2.9a)$$

$$\mathbf{r} \cdot \mathbf{n}_\Omega = 0 \quad \text{on } \Gamma \times (0, T), \quad (2.9b)$$

$$c(\cdot, 0) = c_0 \quad \text{in } \Omega \times \{0\}, \quad (2.9c)$$

where, in $Q_T = \Omega \times (0, T)$, $c = u(w)$ is understood. The change of variable (2.4) and the reformulation (2.9) of the FK problem with variables defined in (2.7) are at the basis of the structure-preserving discretization we introduce in the following section.

We conclude this section by noting that the solution c of the FK problem satisfies the following *entropy stability estimate*, which follows from testing the variational formulation of (2.1) with w , and using (2.5b), (2.8), and the chain rule in (2.6):

$$\int_\Omega s(c(\cdot, \tau)) \, d\mathbf{x} + 4D_0 \int_0^\tau \|\nabla c\|_{L^2(\Omega)^d}^2 \, dt \leq \int_\Omega s(c_0) \, d\mathbf{x} + C_f \|\alpha\|_{L^\infty(\Omega)} \tau |\Omega| \quad \text{for all } 0 < \tau \leq T. \quad (2.10)$$

2.2 The structure-preserving BDF-LDG method

In this section, we present a numerical discretization of the FK problem (2.1) based on formulation (2.9) with auxiliary variables defined in (2.7).

Mesher. We partition the space domain Ω by a locally quasi-uniform polytopic mesh \mathcal{T}_h with mesh size $h := \max_{K \in \mathcal{T}_h} h_K$, where h_K denotes the diameter of the element K . We also partition the time interval $(0, T)$ by a mesh \mathcal{T}_τ defined by the points $0 := t_0 < t_1 < \dots < t_N := T$. For $n = 1, \dots, N$, we define the time interval $I_n := (t_{n-1}, t_n)$ and the time step $\tau_n := t_n - t_{n-1}$.

As usual in the DG setting, we denote the set of all the mesh facets in \mathcal{T}_h by $\mathcal{F}_h = \mathcal{F}_h^I \cup \mathcal{F}_h^N$, where \mathcal{F}_h^I and \mathcal{F}_h^N are the sets of internal and (Neumann) boundary facets, respectively. Additionally, we define the (piecewise constant) mesh-size function $\mathbf{h} \in L^\infty(\mathcal{F}_h^I)$ as

$$\mathbf{h}(\mathbf{x}) := \eta_F^{-1} \left[\frac{1}{2} \left(\left(\frac{|K_1|}{m_{K_1}|F|} \right)^\theta + \left(\frac{|K_2|}{m_{K_2}|F|} \right)^\theta \right) \right]^{1/\theta} \quad \text{if } \mathbf{x} \in F, \text{ and } F \in \mathcal{F}_h^I \text{ is shared by } K_1, K_2 \in \mathcal{T}_h, \quad (2.11)$$

where $\eta_F > 0$ is a parameter independent of the mesh size, which is chosen below in terms of the diffusion tensor and the polynomial degree in the space discretization, θ is the power-mean exponent, and m_{K_*} is the number of facets of the polytopic element K_* . The choice $\theta = 1/2$ in (2.11) is inspired by the definition of the penalty function in [31, §4 and §5]. In the numerical experiments presented below, we use $\theta = -1$ in Section 3 and $\theta = 1/2$ in Section 4.

For each element $K \in \mathcal{T}_h$, let \mathbf{n}_K denote the unit normal vector in d dimensions to ∂K , pointing away from K . Given any piecewise smooth, scalar function μ and any d -vector-valued function $\boldsymbol{\mu}$, we define the

normal jumps and weighted mean values as follows: on each facet $F \in \mathcal{F}_h^I$ shared by two elements K_1 and K_2 of the mesh \mathcal{T}_h , we set

$$\begin{aligned} \llbracket \mu \rrbracket_N &:= \mu|_{K_1} \mathbf{n}_{K_1} + \mu|_{K_2} \mathbf{n}_{K_2}, & \{\!\!\{ \mu \}\!\!\}_{\gamma_F} &:= (1 - \gamma_F) \mu|_{K_1} + \gamma_F \mu|_{K_2}, \\ \llbracket \boldsymbol{\mu} \rrbracket_N &:= \boldsymbol{\mu}|_{K_1} \cdot \mathbf{n}_{K_1} + \boldsymbol{\mu}|_{K_2} \cdot \mathbf{n}_{K_2}, & \{\!\!\{ \boldsymbol{\mu} \}\!\!\}_{\gamma_F} &:= (1 - \gamma_F) \boldsymbol{\mu}|_{K_1} + \gamma_F \boldsymbol{\mu}|_{K_2}, \end{aligned}$$

with $\gamma_F \in [0, 1]$.

For the definition of η_F and γ_F , we follow [32, §2] and set

$$\eta_F = \eta_0 \ell^2 \frac{2(\mathbf{n}_{K_1}^T \mathbf{D}|_{K_1} \mathbf{n}_{K_1})(\mathbf{n}_{K_2}^T \mathbf{D}|_{K_2} \mathbf{n}_{K_2})}{\mathbf{n}_{K_1}^T \mathbf{D}|_{K_1} \mathbf{n}_{K_1} + \mathbf{n}_{K_2}^T \mathbf{D}|_{K_2} \mathbf{n}_{K_2}}, \quad \gamma_F = \frac{\mathbf{n}_{K_1}^T \mathbf{D}|_{K_1} \mathbf{n}_{K_1}}{\mathbf{n}_{K_1}^T \mathbf{D}|_{K_1} \mathbf{n}_{K_1} + \mathbf{n}_{K_2}^T \mathbf{D}|_{K_2} \mathbf{n}_{K_2}},$$

where ℓ is the polynomial degree in the space discretization, and $\eta_0 > 0$ is a constant independent of the problem coefficients and discretization parameters.

DG spaces for the discretization in space. Given a polynomial degree $\ell \in \mathbb{N}$ with $\ell \geq 1$, we define the following spaces:

$$\mathcal{W}^\ell(\mathcal{T}_h) := \prod_{K \in \mathcal{T}_h} \mathbb{P}^\ell(K) \quad \text{and} \quad \mathcal{R}^\ell(\mathcal{T}_h) := \prod_{K \in \mathcal{T}_h} \mathbb{P}^\ell(K)^d,$$

where $\mathbb{P}^\ell(K)$ denotes the space of scalar polynomials of degree at most ℓ defined on K . Additionally, we denote by $\Pi_{\mathcal{W}}$ and $\Pi_{\mathcal{R}}$ the $L^2(\Omega)$ - and $L^2(\Omega)^d$ -orthogonal projections in $\mathcal{W}^\ell(\mathcal{T}_h)$ and $\mathcal{R}^\ell(\mathcal{T}_h)$, respectively.

Discrete differential operators in space. We introduce the discrete space gradient and divergence operators. The LDG gradient operator $\nabla_{\text{LDG}} : \mathcal{W}^\ell(\mathcal{T}_h) \rightarrow \mathcal{R}^\ell(\mathcal{T}_h)$ is defined by

$$(\nabla_{\text{LDG}} v_h, \boldsymbol{\phi}_h)_\Omega = (\nabla_h v_h - \mathcal{L}(v_h), \boldsymbol{\phi}_h)_\Omega \quad \forall \boldsymbol{\phi}_h \in \mathcal{R}^\ell(\mathcal{T}_h),$$

where ∇_h denotes the piecewise gradient operator, and the jump lifting operator $\mathcal{L} : \mathcal{W}^\ell(\mathcal{T}_h) \rightarrow \mathcal{R}^\ell(\mathcal{T}_h)$ is given by

$$(\mathcal{L}(v_h), \boldsymbol{\phi}_h)_\Omega = \sum_{F \in \mathcal{F}_h^I} (\llbracket v_h \rrbracket_N, \{\!\!\{ \boldsymbol{\phi}_h \}\!\!\}_{1-\gamma_F})_F \quad \forall \boldsymbol{\phi}_h \in \mathcal{R}^\ell(\mathcal{T}_h).$$

The LDG divergence operator $\text{div}_{\text{LDG}} : \mathcal{R}^\ell(\mathcal{T}_h) \rightarrow \mathcal{W}^\ell(\mathcal{T}_h)$ is defined by

$$(\text{div}_{\text{LDG}} \mathbf{r}_h, \psi_h)_\Omega = -(\mathbf{r}_h, \nabla_{\text{LDG}} \psi_h)_\Omega \quad \forall \psi_h \in \mathcal{W}^\ell(\mathcal{T}_h).$$

BDF time stepping. We discretize in time with the BDF with ν steps. As for $\nu \geq 7$ the BDF is unstable (see, e.g., [33, Thm. 3.4 in §III.3]), we limit ourselves to $\nu \leq 6$. The notation is as follows: for a nonautonomous ordinary differential equation $y' = g(y, t)$, the ν -step BDF scheme, denoted by BDF ν , reads

$$y^{(n+1)} - \sum_{j=1}^{\nu} a_j(\nu) y^{(n+1-j)} = \tau_{n+1} \beta(\nu) g(y^{(n+1)}, t_{n+1}).$$

From here on, we omit the dependence on ν and simply denote the coefficients β and a_j . For uniform meshes, the coefficients are provided in Table 1. In particular, when $\nu = 1$, the BDF method coincides with the backward Euler method, regardless of the mesh.

The BDF-LDG method. Given a penalty parameter $\varepsilon > 0$, our BDF-LDG discretization of the reformulated FK problem (2.9), after an initialization phase (e.g., using a one-step method, [33, §III.1]), is as follows: for $n = \nu - 1, \dots, N - 1$, find $w_h^{(n+1)} \in \mathcal{W}^\ell(\mathcal{T}_h)$ and $\mathbf{z}_h^{(n+1)}, \boldsymbol{\sigma}_h^{(n+1)}, \mathbf{r}_h^{(n+1)} \in \mathcal{R}^\ell(\mathcal{T}_h)$ (for brevity, we omit the dependence

ν	β	a_1	a_2	a_3	a_4	a_5	a_6
1	1	1					
2	2/3	4/3	-1/3				
3	6/11	18/11	-9/11	2/11			
4	21/25	48/25	-36/25	16/25	-3/25		
5	60/137	300/137	-300/137	200/137	-75/137	12/137	
6	60/147	360/147	-450/147	400/147	-225/147	72/147	-10/147

Table 1: Coefficients of the ν -step BDF with up to $\nu = 6$ for uniform meshes; see, e.g., [34, §3.12].

on ε), such that

$$\mathbf{z}_h^{(n+1)} = -\nabla_{\text{LDG}} w_h^{(n+1)}, \quad (2.12a)$$

$$\left(\mathbf{D}s''(u(w_h^{(n+1)})) \boldsymbol{\sigma}_h^{(n+1)}, \boldsymbol{\phi}_h \right)_\Omega = \left(\mathbf{D}\mathbf{z}_h^{(n+1)}, \boldsymbol{\phi}_h \right)_\Omega \quad \forall \boldsymbol{\phi}_h \in \mathcal{R}^\ell(\mathcal{T}_h), \quad (2.12b)$$

$$\mathbf{r}_h^{(n+1)} = \Pi_{\mathcal{R}}(\mathbf{D}\boldsymbol{\sigma}_h^{(n+1)}), \quad (2.12c)$$

$$\begin{aligned} \varepsilon(w_h^{(n+1)}, \psi_h)_{\text{LDG}} + \frac{1}{\tau_{n+1}\beta} \left(u(w_h^{(n+1)}) - \sum_{j=1}^{\nu} a_j u_h^{(n+1-j)}, \psi_h \right)_\Omega \\ + \left(\text{div}_{\text{LDG}} \mathbf{r}_h^{(n+1)}, \psi_h \right)_\Omega + \sum_{F \in \mathcal{F}_h^I} (\mathbf{h}^{-1} \llbracket w_h^{(n+1)} \rrbracket_{\mathbf{N}}, \llbracket \psi_h \rrbracket_{\mathbf{N}})_F \\ = \left(f(u(w_h^{(n+1)})), \psi_h \right)_\Omega \quad \forall \psi_h \in \mathcal{W}^\ell(\mathcal{T}_h). \end{aligned} \quad (2.12d)$$

In (2.12d), $(\cdot, \cdot)_{\text{LDG}}$ is the bilinear form

$$(w, \psi)_{\text{LDG}} := (\alpha w, \psi)_\Omega + (\mathbf{D}\nabla_{\text{LDG}} w, \nabla_{\text{LDG}} \psi)_\Omega + \sum_{F \in \mathcal{F}_h^I} (\mathbf{h}^{-1} \llbracket w \rrbracket_{\mathbf{N}}, \llbracket \psi \rrbracket_{\mathbf{N}})_F.$$

which is coercive in the norm

$$\|w\|_{\text{DG}}^2 := \|\alpha^{\frac{1}{2}} w\|_{L^2(\Omega)}^2 + \|\mathbf{D}^{\frac{1}{2}} \nabla_h w\|_{L^2(\Omega)^d}^2 + \sum_{F \in \mathcal{F}_h^I} \|\mathbf{h}^{-\frac{1}{2}} \llbracket w \rrbracket_{\mathbf{N}}\|_{L^2(F)}^2.$$

Furthermore, the terms $u_h^{(\kappa)}$ under the summation symbol, which are transmitted from the previous time steps, are defined as follows:

$$u_h^{(\kappa)} := \begin{cases} \Pi_{\mathcal{W}} c_0 & \text{if } \kappa = 0, \\ \Pi_{\mathcal{W}} u(w_h^{(\kappa)}) & \text{if } \kappa > 0, \end{cases}$$

namely, $u_h^{(0)}$ is the $L^2(\Omega)$ projection into $\mathcal{W}^\ell(\mathcal{T}_h)$ of the initial condition for the *original* variable c ; at the subsequent time steps, they are the $L^2(\Omega)$ projections of the *transformed* variables computed at previous time steps.

As $\mathbf{D}s''(u(w))$ is uniformly positive definite, see (2.8), given $w_h^{(n+1)}$ and $\mathbf{z}_h^{(n+1)}$, equation (2.12b) determines $\boldsymbol{\sigma}_h^{(n+1)}$ in a unique way.

Remark 2.1 (Role of the penalty term). *The penalty term with parameter $\varepsilon > 0$ in (2.12d) is introduced to prevent $u(w)$ from getting too close to the extreme values 0 and 1, as the term $s''(\cdot)$ in (2.12b) is singular at those values. Consequently, the penalty term improves the stability and convergence of non-linear solvers such as Newton's method described in Section 2.4.* ■

Remark 2.2 (Discrete entropy stability). *For the lowest-order time stepping BDF1, which coincides with the backward Euler scheme, the fully discrete method (2.12) satisfies the following discrete version of the continuous*

entropy stability estimate (2.10), see [29, Thm. 3.1]:

$$\begin{aligned} \varepsilon \sum_{n=0}^{N-1} \tau_{n+1} \|w_h^{(n+1)}\|_{\text{DG}}^2 + \int_{\Omega} s(u(w_h^{(N)})) \, d\mathbf{x} + 4D_0 \sum_{n=0}^{N-1} \tau_{n+1} \|\boldsymbol{\sigma}_h^{(n+1)}\|_{L^2(\Omega)^d}^2 \\ + \sum_{n=0}^{N-1} \sum_{F \in \mathcal{F}_h^I} \tau_{n+1} \|h^{-\frac{1}{2}} \llbracket w_h^{(n+1)} \rrbracket_{\mathbf{N}}\|_{L^2(F)^d}^2 \leq \int_{\Omega} s(c_0) \, d\mathbf{x} + C_f \|\alpha\|_{L^\infty(\Omega)} |\Omega| T, \end{aligned}$$

with no restrictions on the size of the time steps $\{\tau_n\}_{n=1}^N$. \blacksquare

2.3 Matrix form

In order to write the BDF-LDG method (2.12) in matrix form, we define the following forms and functionals: for all $w_h, \psi_h \in \mathcal{W}^\ell(\mathcal{T}_h)$ and $\mathbf{z}_h, \boldsymbol{\sigma}_h, \boldsymbol{\phi}_h \in \mathcal{R}^\ell(\mathcal{T}_h)$,

$$\begin{aligned} \mathbf{m}_h(\mathbf{z}_h, \boldsymbol{\phi}_h) &:= (\mathbf{z}_h, \boldsymbol{\phi}_h)_\Omega, \\ \mathbf{b}_h(w_h, \boldsymbol{\phi}_h) &:= (\nabla_h v_h, \boldsymbol{\phi}_h)_\Omega - \sum_{F \in \mathcal{F}_h^I} (\llbracket w_h \rrbracket_{\mathbf{N}}, \{\{\boldsymbol{\phi}_h\}\}_{1-\gamma_F})_F, \\ \mathbf{j}_h(w_h, \psi_h) &:= \sum_{F \in \mathcal{F}_h^I} (h^{-1} \llbracket w_h \rrbracket_{\mathbf{N}}, \llbracket \psi_h \rrbracket_{\mathbf{N}})_F, \\ \mathbf{d}_h(w_h, \boldsymbol{\phi}_h) &:= \sum_{K \in \mathcal{T}_h} (\mathbf{D} \mathbf{z}_h, \boldsymbol{\phi}_h)_K, \\ \mathbf{n}_h(w_h; \boldsymbol{\sigma}_h, \boldsymbol{\phi}_h) &:= \sum_{K \in \mathcal{T}_h} (\mathbf{D} s''(u(w_h)) \boldsymbol{\sigma}_h, \boldsymbol{\phi}_h)_K, \\ \mathbf{u}_h(w_h, \psi_h) &:= (u(w_h), \psi_h)_\Omega, \\ \mathbf{f}_h(w_{p,h}, w_{q,h}; \psi_h) &:= (f(u(w_h)), \psi_h)_\Omega. \end{aligned}$$

For fixed bases of $\mathcal{W}^\ell(\mathcal{T}_h)$ and $\mathcal{R}^\ell(\mathcal{T}_h)$, we denote by $\mathbf{W}_h, \mathbf{Z}_h, \boldsymbol{\Sigma}_h$, and \mathbf{R}_h the coefficient vectors expressing $w_h, \mathbf{z}_h, \boldsymbol{\sigma}_h$, and \mathbf{r}_h , respectively, in terms of those bases. Additionally, we denote by M_I, B, J, M_D , and A_{LDG} the matrices associated with the bilinear forms $\mathbf{m}_h(\cdot, \cdot), \mathbf{b}_h(\cdot, \cdot), \mathbf{j}_h(\cdot, \cdot), \mathbf{d}_h(\cdot, \cdot)$, and $(\cdot, \cdot)_{\text{LDG}}$, respectively, and by \mathcal{N}, \mathcal{U} , and \mathcal{F} the operators associated with the non-linear functionals $\mathbf{n}_h(\cdot; \cdot, \cdot), \mathbf{u}_h(\cdot, \cdot)$, and $\mathbf{f}_h(\cdot, \cdot; \cdot)$ respectively. Since the non-linear functional $\mathbf{n}_h(\cdot; \cdot, \cdot)$ is linear with respect to its second argument, we write $\mathcal{N}(\mathbf{W}_h^{(n+1)}; \boldsymbol{\Sigma}_h^{(n+1)})$ instead of $\mathcal{N}(\mathbf{W}_h^{(n+1)}; \boldsymbol{\Sigma}_h^{(n+1)})$.

Then, the matrix form of the method in (2.12) is as follows:

$$M_I \mathbf{Z}_h^{(n+1)} = -B \mathbf{W}_h^{(n+1)}, \quad (2.13a)$$

$$\mathcal{N}(\mathbf{W}_h^{(n+1)}; \boldsymbol{\Sigma}_h^{(n+1)}) = M_D \mathbf{Z}_h^{(n+1)}, \quad (2.13b)$$

$$M_I \mathbf{R}_h^{(n+1)} = M_D \boldsymbol{\Sigma}_h^{(n+1)}, \quad (2.13c)$$

$$\varepsilon A_{\text{LDG}} \mathbf{W}_h^{(n+1)} + \frac{1}{\tau_{n+1} \beta} \mathcal{U}(\mathbf{W}_h^{(n+1)}) - B^T \mathbf{R}_h^{(n+1)} + J \mathbf{W}_h^{(n+1)} = \mathcal{F}(\mathbf{W}_h^{(n+1)}) + \frac{1}{\tau_{n+1} \beta} \sum_{j=1}^{\nu} a_j \mathcal{U}_h^{(n+1-j)}, \quad (2.13d)$$

where, in (2.13d), the terms $\mathcal{U}_h^{(\kappa)}$ under the summation symbol represent the coefficient vector of $\Pi_{\mathcal{W}} p_0$ if $\kappa = 0$, and $\mathcal{U}_h^{(\kappa)} := \mathcal{U}(\mathbf{W}_h^{(\kappa)})$ if $\kappa > 0$.

As the mass matrix M_I is symmetric, positive definite, and block diagonal, it can be inverted efficiently and we can write

$$\mathbf{Z}_h^{(n+1)} = -M_I^{-1} B \mathbf{W}_h^{(n+1)} \quad \text{and} \quad \mathbf{R}_h^{(n+1)} = M_I^{-1} M_D \boldsymbol{\Sigma}_h^{(n+1)}.$$

Then, system (2.13) reduces to

$$\mathcal{N}(\mathbf{W}_h^{(n+1)}; \boldsymbol{\Sigma}_h^{(n+1)}) = -M_D M_I^{-1} B \mathbf{W}_h^{(n+1)}, \quad (2.14a)$$

$$\varepsilon A_{\text{LDG}} \mathbf{W}_h^{(n+1)} + \frac{1}{\tau_{n+1} \beta} \mathcal{U}(\mathbf{W}_h^{(n+1)}) - B^T M_I^{-1} M_D \boldsymbol{\Sigma}_h^{(n+1)} + J \mathbf{W}_h^{(n+1)} = \mathcal{F}(\mathbf{W}_h^{(n+1)}) + \frac{1}{\tau_{n+1} \beta} \sum_{j=1}^{\nu} a_j \mathcal{U}_h^{(n+1-j)}. \quad (2.14b)$$

Remark 2.3 (Reduced system with one unknown). Given $\mathbf{W}_h^{(n+1)}$, equation (2.14a) determines $\boldsymbol{\Sigma}_h^{(n+1)}$ in a unique way. This follows from the uniform positive definiteness of $\mathbf{D}s''(u(w))$; see (2.8). Then, using $\boldsymbol{\Sigma}_h^{(n+1)} = -(\mathcal{N}(\mathbf{W}_h^{(n+1)}))^{-1} M_D M_I^{-1} B \mathbf{W}_h^{(n+1)}$, system (2.14) can be reformulated in the $\mathbf{W}_h^{(n+1)}$ unknown only as

$$\begin{aligned} \varepsilon A_{\text{LDG}} \mathbf{W}_h^{(n+1)} + \frac{1}{\tau_{n+1}\beta} \mathcal{U}(\mathbf{W}_h^{(n+1)}) + B^T M_I^{-1} M_D (\mathcal{N}(\mathbf{W}_h^{(n+1)}))^{-1} M_D M_I^{-1} B \mathbf{W}_h^{(n+1)} + J \mathbf{W}_h^{(n+1)} \\ = \mathcal{F}(\mathbf{W}_h^{(n+1)}) + \frac{1}{\tau_{n+1}\beta} \sum_{j=1}^{\nu} a_j \mathcal{U}_h^{(n+1-j)}. \end{aligned} \quad (2.15)$$

■

2.4 Newton's iteration

To complete the presentation of the method, we derive explicitly the linear systems stemming from Newton's iteration. One of the most computationally expensive parts in each linear iteration is the evaluation of the non-linear terms in the multivariate function and its Jacobian matrix. However, since non-linearities in our method do not appear on interface integrals, these terms can be computed independently for each element K of \mathcal{T}_h , and their corresponding Jacobians are block diagonal. Consequently, our method has an inherent parallelizable structure.

We set, for convenience, $C := M_D M_I^{-1} B$ and

$$\begin{aligned} \mathcal{G}_1(\boldsymbol{\Sigma}_h^{(n+1)}, \mathbf{W}_h^{(n+1)}) &:= \mathcal{N}(\mathbf{W}_h^{(n+1)}) \boldsymbol{\Sigma}_h^{(n+1)} + C \mathbf{W}_h^{(n+1)}, \\ \mathcal{G}_2(\boldsymbol{\Sigma}_h^{(n+1)}, \mathbf{W}_h^{(n+1)}) &:= \varepsilon A_{\text{LDG}} \mathbf{W}_h^{(n+1)} + \frac{1}{\tau_{n+1}\beta} \mathcal{U}(\mathbf{W}_h^{(n+1)}) - C^T \boldsymbol{\Sigma}_h^{(n+1)} + J \mathbf{W}_h^{(n+1)} \\ &\quad - \mathcal{F}(\mathbf{W}_h^{(n+1)}) - \frac{1}{\tau_{n+1}\beta} \sum_{j=1}^{\nu} \mathcal{U}_h^{(n+1-j)}. \end{aligned}$$

Denote by $\mathcal{D}_{\boldsymbol{\Sigma}}$ and $\mathcal{D}_{\mathbf{W}}$ the differential operators with respect to $\boldsymbol{\Sigma}$ and \mathbf{W} , respectively. Omitting the temporal index $n+1$, the step $k \rightarrow k+1$ of Newton's iteration applied to system (2.14) reads as follows:

$$\begin{aligned} \mathcal{D}_{\boldsymbol{\Sigma}}(\mathcal{G}_1(\boldsymbol{\Sigma}_h^k, \mathbf{W}_h^k)) (\boldsymbol{\Sigma}_h^{k+1} - \boldsymbol{\Sigma}_h^k) + \mathcal{D}_{\mathbf{W}}(\mathcal{G}_1(\boldsymbol{\Sigma}_h^k, \mathbf{W}_h^k)) (\mathbf{W}_h^{k+1} - \mathbf{W}_h^k) &= -\mathcal{G}_1(\boldsymbol{\Sigma}_h^k, \mathbf{W}_h^k), \\ \mathcal{D}_{\boldsymbol{\Sigma}}(\mathcal{G}_2(\boldsymbol{\Sigma}_h^k, \mathbf{W}_h^k)) (\boldsymbol{\Sigma}_h^{k+1} - \boldsymbol{\Sigma}_h^k) + \mathcal{D}_{\mathbf{W}}(\mathcal{G}_2(\boldsymbol{\Sigma}_h^k, \mathbf{W}_h^k)) (\mathbf{W}_h^{k+1} - \mathbf{W}_h^k) &= -\mathcal{G}_2(\boldsymbol{\Sigma}_h^k, \mathbf{W}_h^k). \end{aligned}$$

We compute

$$\begin{aligned} \mathcal{D}_{\boldsymbol{\Sigma}}(\mathcal{G}_1(\boldsymbol{\Sigma}_h^k, \mathbf{W}_h^k)) &= \mathcal{N}(\mathbf{W}_h^k), \\ \mathcal{D}_{\mathbf{W}}(\mathcal{G}_1(\boldsymbol{\Sigma}_h^k, \mathbf{W}_h^k)) &= \mathcal{D}_{\mathbf{W}}(\mathcal{N}(\mathbf{W}_h^k)) \boldsymbol{\Sigma}_h^k + C, \\ \mathcal{D}_{\boldsymbol{\Sigma}}(\mathcal{G}_2(\boldsymbol{\Sigma}_h^k, \mathbf{W}_h^k)) &= -C^T, \\ \mathcal{D}_{\mathbf{W}}(\mathcal{G}_2(\boldsymbol{\Sigma}_h^k, \mathbf{W}_h^k)) &= \varepsilon A_{\text{LDG}} + \frac{1}{\tau_{n+1}\beta} \mathcal{D}_{\mathbf{W}}(\mathcal{U}(\mathbf{W}_h^k)) + J - \mathcal{D}_{\mathbf{W}}(\mathcal{F}(\mathbf{W}_h^k)). \end{aligned}$$

Therefore, the Newton iteration applied to system (2.14) is as follows:

$$\begin{aligned} \mathcal{N}(\mathbf{W}_h^k) \boldsymbol{\Sigma}_h^{k+1} &= -\left[\mathcal{D}_{\mathbf{W}}(\mathcal{N}(\mathbf{W}_h^k)) \boldsymbol{\Sigma}_h^k + C \right] \mathbf{W}_h^{k+1} + (\mathcal{D}_{\mathbf{W}}(\mathcal{N}(\mathbf{W}_h^k)) \boldsymbol{\Sigma}_h^k) \mathbf{W}_h^k, \\ -C^T \boldsymbol{\Sigma}_h^{k+1} + \left[\varepsilon A_{\text{LDG}} + \frac{1}{\tau_{n+1}\beta} \mathcal{D}_{\mathbf{W}}(\mathcal{U}(\mathbf{W}_h^k)) + J - \mathcal{D}_{\mathbf{W}}(\mathcal{F}(\mathbf{W}_h^k)) \right] \mathbf{W}_h^{k+1} \\ &= \left[\frac{1}{\tau_{n+1}\beta} \mathcal{D}_{\mathbf{W}}(\mathcal{U}(\mathbf{W}_h^k)) - \mathcal{D}_{\mathbf{W}}(\mathcal{F}(\mathbf{W}_h^k)) \right] \mathbf{W}_h^k - \frac{1}{\tau_{n+1}\beta} \left[\mathcal{U}(\mathbf{W}_h^k) - \sum_{j=1}^{\nu} \mathcal{U}_h^{(n+1-j)} \right] + \mathcal{F}(\mathbf{W}_h^k). \end{aligned} \quad (2.16)$$

Remark 2.4 (Newton’s iteration for (2.15)). *Using (2.14a), one can eliminate Σ_h^k from (2.16) and obtain*

$$\begin{aligned} & \left[\varepsilon A_{\text{LDG}} + \frac{1}{\tau_{n+1}\beta} \mathcal{D}_{\mathbf{W}}(\mathcal{U}(\mathbf{W}_h^k)) + C^T (\mathcal{N}(\mathbf{W}_h^k))^{-1} C - \mathbb{M}\mathbf{W}_h^k + J - \mathcal{D}_{\mathbf{W}}(\mathcal{F}(\mathbf{W}_h^k)) \right] \mathbf{W}_h^{k+1} \\ & = \left[\frac{1}{\tau_{n+1}\beta} \mathcal{D}_{\mathbf{W}}(\mathcal{U}(\mathbf{W}_h^k)) - \mathcal{D}_{\mathbf{W}}(\mathcal{F}(\mathbf{W}_h^k)) - (\mathbb{M}\mathbf{W}_h^k) \right] \mathbf{W}_h^k - \frac{1}{\tau_{n+1}\beta} \left[\mathcal{U}(\mathbf{W}_h^k) - \sum_{j=1}^{\nu} \mathcal{U}_h^{(n+1-j)} \right] + \mathcal{F}(\mathbf{W}_h^k), \end{aligned} \quad (2.17)$$

where \mathbb{M} is the third-order tensor defined as

$$\mathbb{M} := C^T (\mathcal{N}(\mathbf{W}_h^k))^{-1} \mathcal{D}_{\mathbf{W}}(\mathcal{N}(\mathbf{W}_h^k)) (\mathcal{N}(\mathbf{W}_h^k))^{-1} C.$$

The expression in (2.17) can also be obtained by applying Newton’s iteration directly to the reformulation of system (2.14) given in (2.15). \blacksquare

3 Numerical verification

In this section, we present some numerical tests to assess the accuracy of the proposed structure-preserving LDG method. We consider test cases in two space dimensions. In Section 3.1, we discuss the convergence properties of the scheme in space and time for a smooth exact solution. Then, in Section 3.2, we study the accuracy of the method in simulating a traveling-wave solution, providing a comparison with an existing interior penalty DG (IPDG) method that does not guarantee the positivity preservation [19]. All numerical simulations in this section are based on the `lymph` library [35], implementing DG methods on polytopic meshes. The polygonal meshes are constructed using PolyMesher [36]. All the constructed meshes satisfy the polytopic regularity assumptions of [17, Assumption 30 in §4.3]. We use time meshes with uniform time step τ .

Since the elements in the meshes we use in this section have a uniformly small number of edges, we neglect the dependence of the mesh-size function h in (2.11) on m_{K_*} . We fix $\theta = -1$ in (2.11), and set the stabilization parameter $\eta_0 = 1$ in the definition of η_F . For the Newton iterations, given a small tolerance tol , we adopt the following stopping criterion:

$$\min \{ \|w_h^{k+1} - w_h^k\|_{L^2(\Omega)}, |\text{res}_{k+1}| \} \leq \text{tol}, \quad (3.1)$$

where res_{k+1} is the residual of the algebraic system (2.15) for the approximation at the $(k+1)$ th Newton’s iteration of $w_h^{(n+1)}$. In the convergence tests reported below, we measure the errors at the final time

$$E_c := \|c(\cdot, T) - u(w_h^{(N)})\|_{L^2(\Omega)} \quad \text{and} \quad E_{\sigma} := \|\nabla c(\cdot, T) + \sigma_h^{(N)}\|_{L^2(\Omega)^d}.$$

3.1 Test case 1: Convergence analysis

For the numerical tests in this section, we consider the space domain $\Omega = (0, 1)^2$ and homogeneous Neumann boundary conditions on $\Gamma \times (0, T)$. For the non-linear Newton solver, we use the stopping criteria (3.1) with $\text{tol} = 10^{-16}$. The penalty parameter ε is set to 0.

Convergence properties of the space discretization

For this test, we use the BDF1 time-stepping scheme (implicit Euler) for the time discretization. We select the diffusion tensor $\mathbf{D} = \mathbb{I}_2$, where \mathbb{I}_2 represents the identity matrix of size 2, and the reaction coefficient $\alpha = 1$, and consider the FK equation with an additional source term on the right-hand side so that problem (2.1) admits the following manufactured exact solution:

$$c(x, y, t) = \frac{1}{4} (\cos(2\pi x) \cos(2\pi y) + 2) (1 - t).$$

The choice of a solution that is linear in time allows us to neglect the error due to the BDF scheme, highlighting the properties of the space discretization.

We perform a convergence test keeping fixed the polynomial degree of the space approximation $\ell = 1, 2, 3, 4$ and using, for each degree, different mesh refinements with number of elements ($N_{\text{el}} = 30, 100, 300, 1000$). The polygonal meshes used in this test case are reported in Figure 1. We take $\tau = 10^{-3}$ and a final time

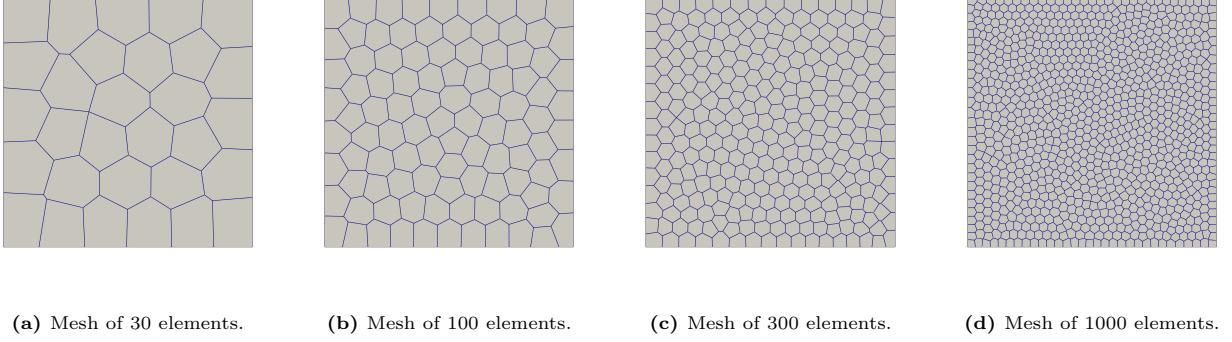


Figure 1: Test case 1: meshes with different levels of refinement used in the h -convergence test.

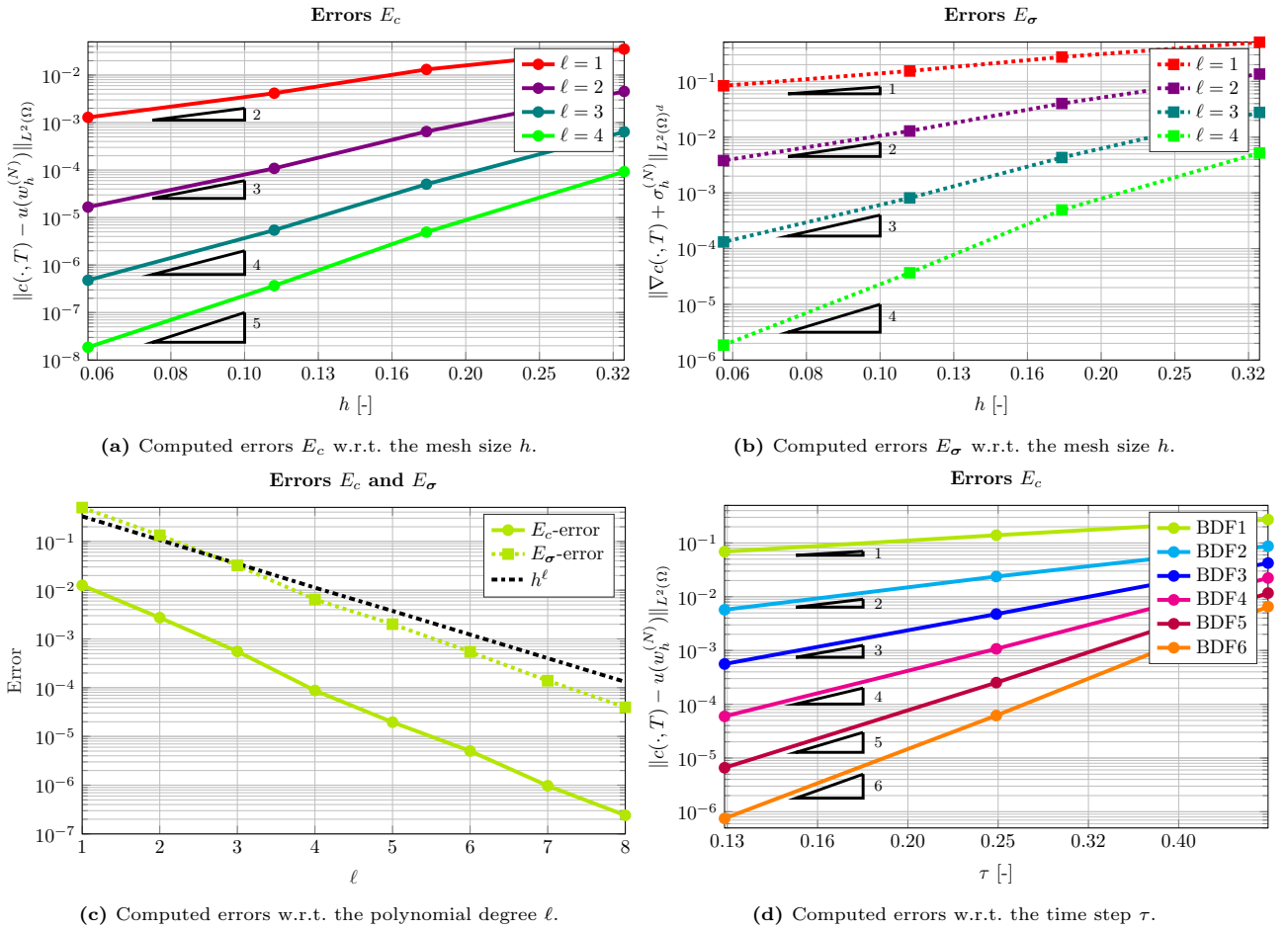


Figure 2: Test case 1: computed errors and convergence rates.

$T = 5 \times 10^{-2}$. In Figures 2a and 2b, we report the computed errors E_c and E_σ . We observe a decrease in the error with quasi-optimal convergence, namely, of order $\mathcal{O}(h^\ell)$ for E_σ , and of order $\mathcal{O}(h^{\ell+1})$ for E_c .

Then, we develop a convergence analysis with respect to the polynomial degree ℓ . In this case, we consider a coarse mesh with 30 polygonal elements, and we take $\tau = 10^{-5}$ and $T = 2.5 \times 10^{-4}$. The errors E_c and E_σ are reported in Figure 2c, where we also report the line of convergence rate h^ℓ . Comparing the results, we can observe a spectral convergence in the polynomial degree ℓ .

Convergence properties of the time discretization

We also test the convergence in time of the fully discrete scheme by comparing the six stable BDF schemes. For this test, we select the diffusion tensor $\mathbf{D} = 10^{-3}\mathbb{I}_2$ and the reaction coefficient $\alpha = 1$, and we slightly modify the time dependence in the manufactured exact solution with respect to the previous experiment to highlight the properties of the time discretization:

$$c(x, y, t) = \frac{1}{4} (\cos(2\pi x) \cos(2\pi y) + 2) e^{-t}.$$

We use a fixed mesh of 300 elements ($h \approx 0.1097$) and a polynomial degree $\ell = 4$ for the space discretization. This guarantees that the errors induced by the space discretization are sufficiently small to highlight the convergence properties of the time integration methods.

The convergence test uses three different time steps $\tau = 0.500, 0.250, 0.125$, and a final time $T = 2$. In Figure 2d, we report the computed errors E_c . Coherently with the theoretical results on BDF methods, we observe a decrease in the error of order $\mathcal{O}(\tau^\nu)$ for the general BDF $_\nu$ method.

3.2 Test case 2: Traveling-wave solution

In this section, we emphasize the critical role of the strong positivity-preserving property of the BDF-LDG formulation (2.14) in accurately simulating a traveling-wave solution. We fix an anisotropic diffusion tensor $\mathbf{D} = d_{\text{ext}}\mathbb{I}_2$ and a constant reaction coefficient α , and we consider a solution of the form

$$c(x, y, t) = \psi(x - vt) = \psi(\xi),$$

where v is wave speed depending on d_{ext} and α defined by $v := 5\sqrt{\alpha d_{\text{ext}}/6}$. Substituting c in the FK equation, we obtain the following equivalent system of ordinary differential equations:

$$\begin{cases} \chi'(\xi) = -\frac{v}{d_{\text{ext}}}\chi(\xi) + \frac{\alpha}{d_{\text{ext}}}\psi(\xi)(\psi(\xi) - 1) & \xi \in (0, T), \\ \psi'(\xi) = \chi(\xi) & \xi \in (0, T). \end{cases} \quad (3.2)$$

The analytical solution of problem (3.2) is given by (see [37, §7.2])

$$\psi(\xi) = \frac{1}{4} \left(1 + \tanh \left(8 - \sqrt{\frac{\alpha}{24d_{\text{ext}}}} \xi \right) \right)^2.$$

This solution satisfies a homogeneous Neumann boundary condition at the limits $\xi \rightarrow \pm\infty$, which is equivalent to $x \rightarrow \pm\infty$ for each fixed value of $t \in (0, T)$. The homogeneous Neumann boundary condition is also respected in the y -direction, as the exact solution c is independent of y . In this simulation, we consider a rectangular space domain $\Omega = (0, 3) \times (0, 1)$, and the final time $T = 10$. We impose homogeneous Neumann boundary conditions not only at $y = 0$ and $y = 1$, but also at $x = 0$ and $x = 3$.

Concerning the physical parameters, we fix $d_{\text{ext}} = 10^{-3}$ and $\alpha = 1$, with associated velocity $v \simeq 6.45 \times 10^{-2}$. For the non-linear Newton solver, we use the stopping criteria (3.1) with $\text{tol} = 10^{-10}$.

Impact of the penalty parameter ε

In the first test, we analyze the impact of the penalty parameter ε on the error convergence. To test this, we fix the polynomial degree $\ell = 5$, and the mesh consisting of 50 elements generated with PolyMesher [36]. We consider as time step $\tau = 2.5 \times 10^{-2}$, and as final time $T = 10$. In this case, we test two different choices of BDF $_\nu$ scheme, namely, $\nu = 1$ and $\nu = 6$.

As we can observe in Figure 3a, increasing the penalty parameter introduces an error that seems to be of order $\mathcal{O}(\varepsilon)$. Such a behavior is especially evident in the case of the BDF6 discretization. For the BDF1 scheme, a plateau is observed due to the dominance of the time discretization error. In [29, §5.1], it was proven that the mass loss due to the penalty term is of order $\mathcal{O}(\varepsilon^{\frac{1}{2}})$; however, an order $\mathcal{O}(\varepsilon)$ was numerically observed. Therefore, as the introduction of the penalty term increases the error of the method, it should be used only when it is necessary to get convergence of the non-linear Newton solver (see Remark 2.1). For this reason, in the next steps of this test case, we fix $\varepsilon = 0$, as the penalty term does not seem to be necessary.

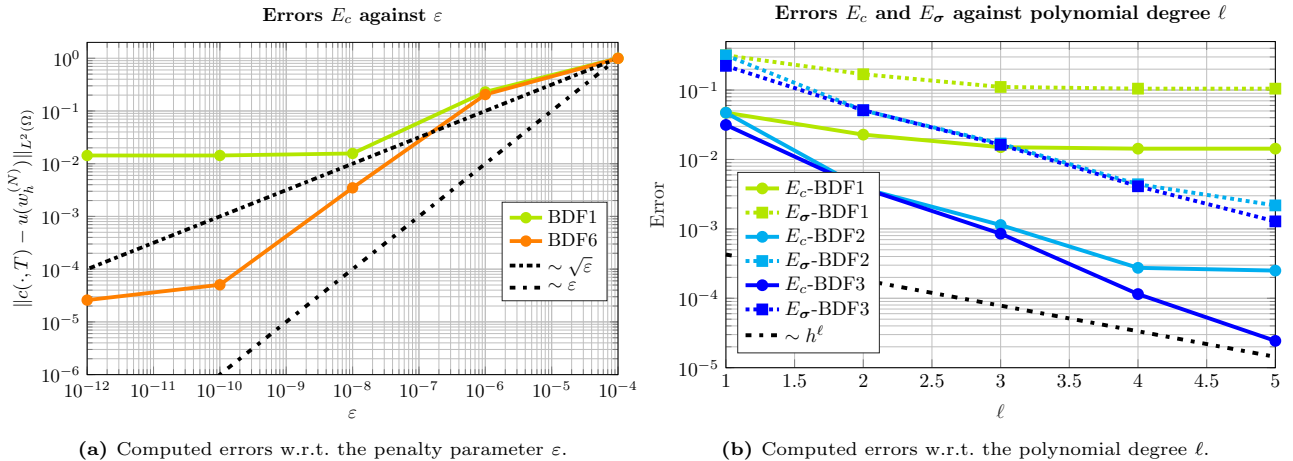


Figure 3: Test case 2: computed errors w.r.t. the penalty parameter ε (a), and w.r.t. the polynomial degree ℓ (b).

Convergence with respect to the polynomial degree ℓ

In the second test, we analyze the convergence with respect to the polynomial degree ℓ for different choices of BDF ν scheme ($\nu = 1, \dots, 6$). We use a fixed mesh consisting of 50 elements generated with PolyMesher [36], and consider as time step $\tau = 2.5 \times 10^{-2}$ and as final time $T = 10$.

We report in Figure 4 the numerical solutions obtained with different choices of the polynomial degree ℓ , $\ell = 1, \dots, 5$, and with the BDF6 scheme for the time discretization. On the first row, we report the initial condition at time $t = 0$. As shown, the choice of using an $L^2(\Omega)$ -projection of the field $c_0(\mathbf{x})$ can result in a highly discontinuous approximation and. Locally, this can cause the values to fall outside the range $(0, 1)$, particularly for low polynomial degrees. However, the transformation in (2.4) ensures that the solution values are pointwise within $(0, 1)$ from the very first time step. As shown in the second row, the method provides an accurate representation of the wavefront propagation.

In Figure 3b, we report the errors E_c and E_σ . We observe that using a higher-order time-stepping scheme results in spectral convergence in ℓ . In contrast, the BDF1 and BDF2 schemes lead to error stagnation, which cannot be reduced by improving the space discretization, as the time discretization error dominates in such cases. We do not report the errors of BDF ν methods for $\nu=4, 5, 6$ as their performance in this test case is identical to that of the BDF3 scheme.

Convergence with respect to the space mesh size h

In the third test, we analyze the convergence with respect to the space mesh size h for different choices of the BDF ν scheme ($\nu = 1, \dots, 6$). We fix two different polynomial degrees of approximation, $\ell = 2$ and $\ell = 3$, and test on a sequence of meshes consisting of 50, 100, 200, 400, 800, 1600 elements generated with PolyMesher [36]. We take as final time $T = 1$, and a fixed time step $\tau = 10^{-1}$ and use high-order BDF ν time stepping schemes to let the space error dominate.

In Figures 5a and 5c, we report the errors E_c and E_σ , respectively, for $\ell = 2$. Additionally, in Figures 5b and 5d, we report the errors E_c and E_σ for $\ell = 3$. For sufficiently high-order time stepping schemes, we can observe that the errors E_c and E_σ decay with optimal orders $\mathcal{O}(h^{\ell+1})$ and $\mathcal{O}(h^\ell)$, respectively. In contrast, low-order BDF schemes cause error stagnation, as the time discretization error dominates over the error in space. For the chosen mesh refinements, the correct slope can be found using the BDF4 scheme for $\ell = 2$, but it requires a BDF5 for $\ell = 3$. In Figure 5, we do not report the results for BDF ν schemes of higher order, as they do not improve significantly the accuracy of the method. This experiment also emphasizes the *unconditional stability* of the method, meaning that there is no need to choose a time step sufficiently small with respect to the space mesh size to prevent blow-up of the numerical solution.

Comparison with an interior penalty DG method

Finally, we compare the results obtained with our method and the ones obtained with another method proposed in the literature. In particular, we focus on an IPDG method proposed in [19]. This method is not positivity-

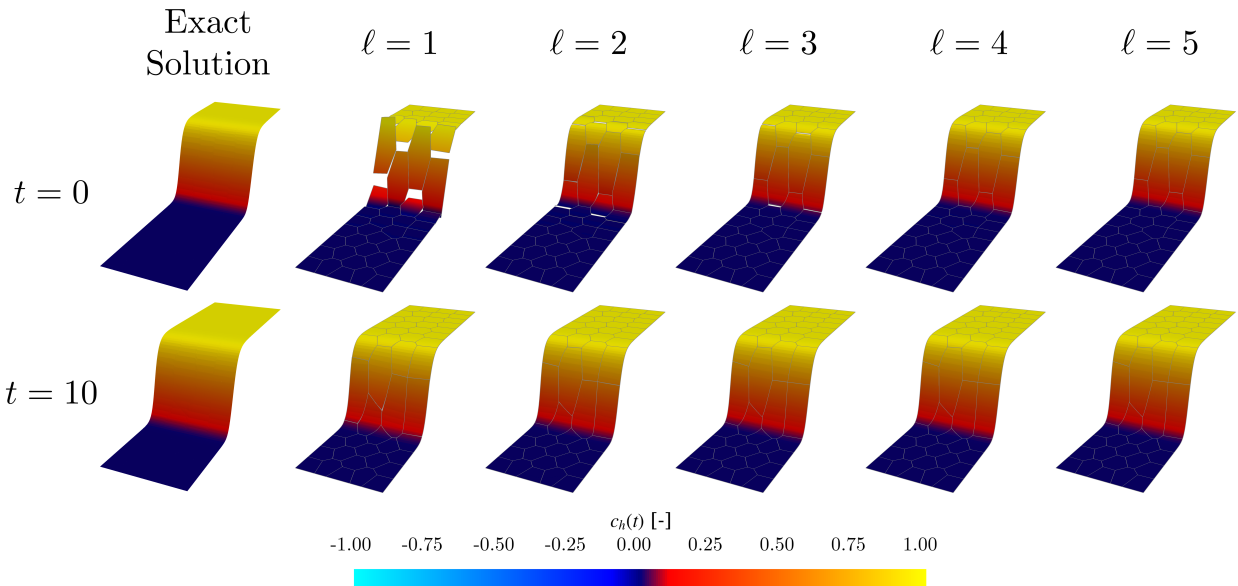


Figure 4: Test case 2: Comparison of initial conditions and solutions of wave propagation problem for different polynomial degrees $\ell = 1, \dots, 5$ at different times $t = 0, 10$.

preserving, but if the mesh size is sufficiently fine or the polynomial degree is sufficiently high, the analytical solution is approximated correctly.

For this test, we use two meshes with 50 and 200 elements and different polynomial degrees $\ell = 1, \dots, 5$. We consider as time step $\tau = 2.5 \times 10^{-2}$ and as final time $T = 10$. As for the time discretization, we adopt the BDF1 and BDF2 schemes for our structure-preserving LDG method. The results are compared with those obtained with the implicit Euler scheme (BDF1) and the Crank-Nicolson scheme (of order 2) for the IPDG approach proposed in [19]. This ensures that, in the comparison, the two space discretizations are paired with time stepping schemes of the same orders.

In Figure 6, we report the results obtained for a mesh with 50 elements, using the time integration schemes of the second-order. We observe that, using the IPDG method, the solution does not maintain positivity and takes negative values at certain points, thereby losing physical meaning. This issue can be mitigated by increasing the degree ℓ of the approximation in space. In contrast, our method remains free of oscillations and preserves the pointwise bounds of the continuous solution.

To quantify the quality of the numerical approximation obtained with the two methods, we report in Table 2 the errors in the $L^2(\Omega)$ norm, namely $\|c(\cdot, T) - u(w_h^{(N)})\|_{L^2(\Omega)}$ for the structure-preserving LDG method and $\|c(\cdot, T) - c_h^{(N)}\|_{L^2(\Omega)}$ for the IPDG method. This shows that the method proposed in [19] only approximates the exact solution accurately when a sufficiently large number of degrees of freedom are used. This requires increasing the accuracy in space (by either increasing ℓ or reducing h), which appears to be more crucial than reducing the time step. In contrast, our method is not affected by these issues and can capture the solution correctly even with low-order polynomial degrees. The performance of both methods becomes comparable for higher-order approximations.

4 Spreading of α -synuclein in a two-dimensional brain section

In this section, we present some numerical simulations of the spreading of α -synuclein, conducted using our structure-preserving LDG method. The aggregation, phosphorylation, and nitration of this synaptic protein have been suggested to be critical processes in forming aggregates known as Lewy bodies. These lesions are associated with several neurodegenerative diseases, including Parkinson's disease (PD), dementia with Lewy bodies (DLB), incidental Lewy body disease (ILBD), and Alzheimer's disease with Lewy bodies (ADLB) [38]. All these conditions share a common developmental process described in the literature by the Unified Staging System for Lewy Body Disorders (USSLB) [3, 39]. This theory divides pathological spreading of α -synuclein

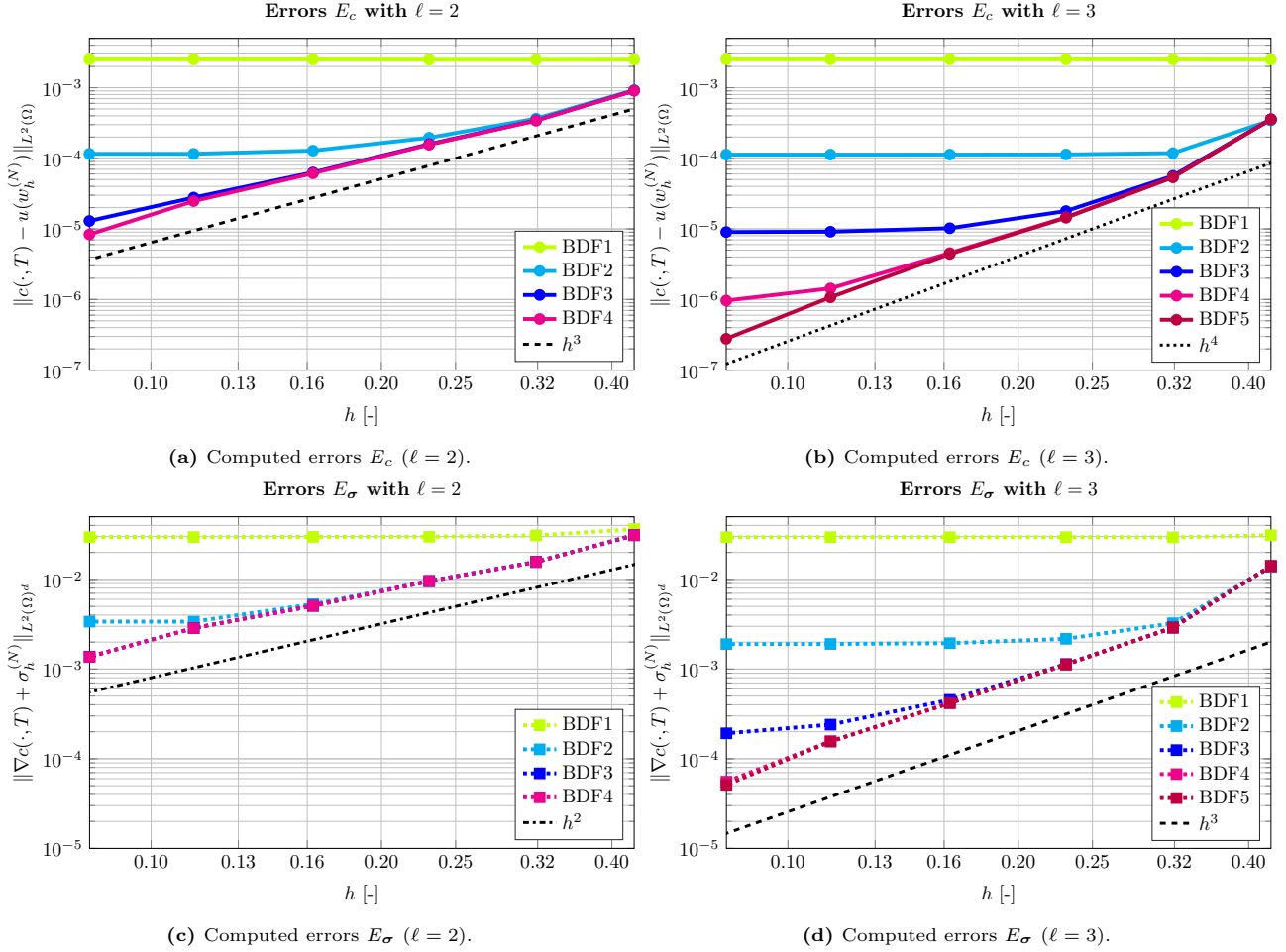


Figure 5: Test case 2: computed errors and convergence rates.

into 4 stages, but with two distinct patterns that may emerge at the prodromal stage: primarily brainstem inclusions (most common in PD) or limbic inclusions (typical in DLB, ADLB) [39].

In the literature, the mathematical modeling of these processes typically uses the *heterodimer model* [2, 20, 40, 41], which describes the evolution of the healthy protein concentration p and the misfolded protein concentration q . Denoting as $\kappa_p > 0$ the production rate of p , $\lambda_p > 0$ and $\lambda_q > 0$ the clearance rates of p and q , respectively, and $\mu_{pq} > 0$ the conversion rate from p to q , the heterodimer system with initial conditions and open boundary conditions reads as follows:

$$\begin{aligned}
 \partial_t p - \nabla \cdot (\mathbf{D} \nabla p) &= -p(\lambda_p + \mu_{pq} q) + \kappa_p && \text{in } Q_T, \\
 \partial_t q - \nabla \cdot (\mathbf{D} \nabla q) &= -q(\lambda_q - \mu_{pq} p) && \text{in } Q_T, \\
 (\mathbf{D} \nabla p) \cdot \mathbf{n}_\Omega &= 0 \text{ and } (\mathbf{D} \nabla q) \cdot \mathbf{n}_\Omega = 0 && \text{on } \Gamma \times (0, T), \\
 p(\cdot, 0) &= p_0 \text{ and } q(\cdot, 0) = q_0 && \text{in } \Omega.
 \end{aligned}$$

Assuming constant coefficients and $p \gg q$, and neglecting the time derivative and diffusion of p , p can be computed in terms of q as $p = \frac{\kappa_p}{\lambda_p + \mu_{pq} q}$. By performing a Taylor expansion, $p \simeq \frac{\kappa_p}{\lambda_p} \left(1 - \frac{\mu_{pq}}{\lambda_p} q\right)$. Substituting this into the second equation of the heterodimer system, and setting $c := q/q_M$, with $q_M := \lambda_p(\kappa_p \mu_{pq} - \lambda_p \lambda_q) / (\kappa_p \mu_{pq}^2)$, one obtains the FK equation with $\alpha = (\kappa_p \mu_{pq} - \lambda_p \lambda_q) / \lambda_p$; see [2]. Under these assumptions, the FK equation in (2.1) can be viewed as a simplified version of the heterodimer model, applicable when the dynamics of the healthy protein population are negligible. Indeed, the FK equation has been widely used in the literature to model and simulate the spreading of proteins in neurodegenerative diseases [19, 40].

Here, we simulate the spreading of α -synuclein in both prodromal stages, modeled by the FK equation to analyze the evolution in a simplified 2D geometry. The brain geometry is segmented starting from a structural

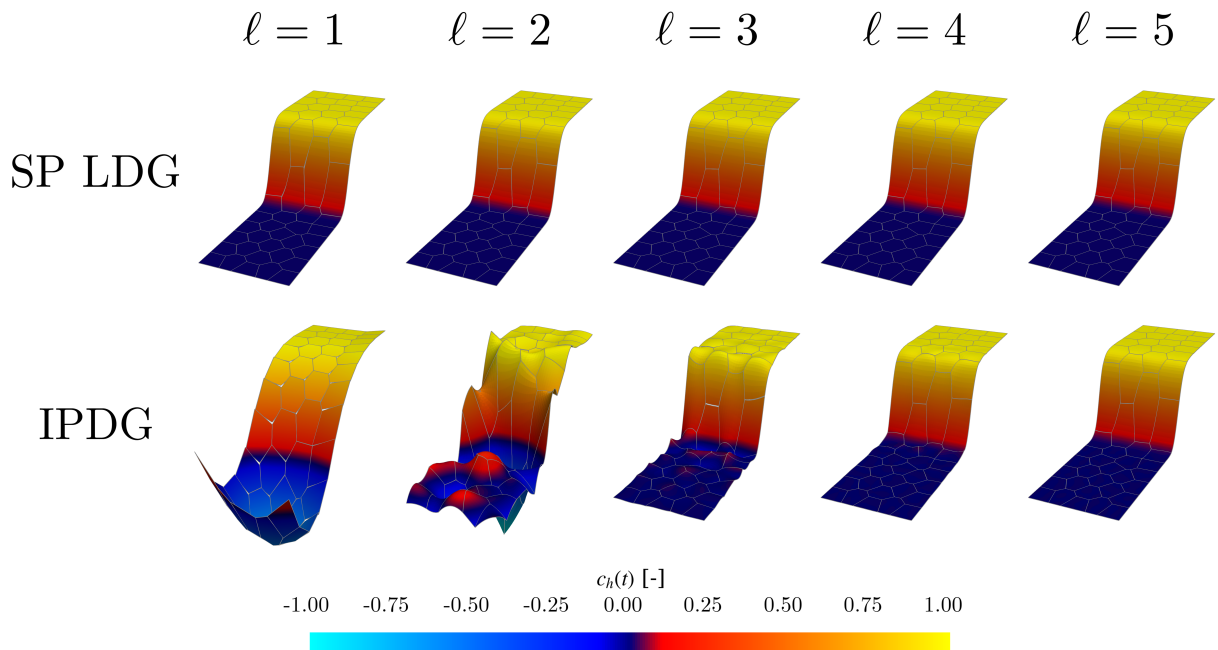


Figure 6: Test case 2: Comparison solutions at time $t = 3$ for different polynomial degrees $\ell = 1, \dots, 5$ and computed with different methods: the structure-preserving LDG (first line) and the IPDG (second line).

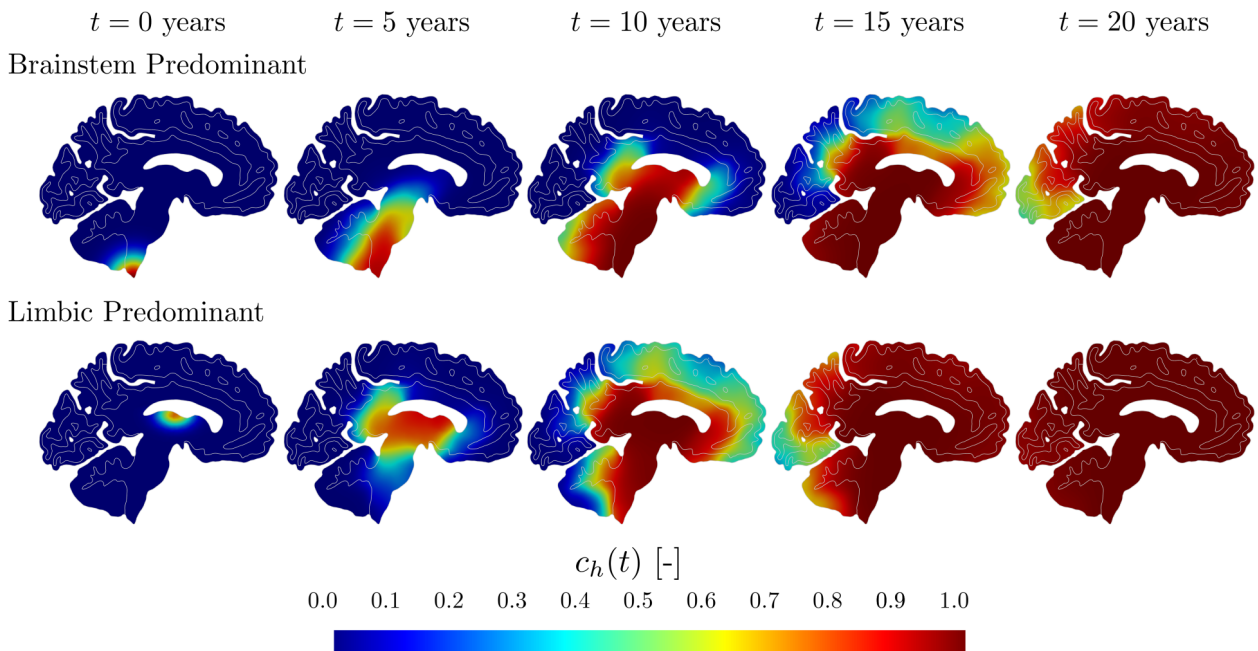


Figure 7: Test case 3: Patterns of α -synuclein concentration at different stages of the pathology.

magnetic resonance image of a brain from the OASIS-3 database [42]. We construct a polygonal agglomerated grid of a sagittal 2D brain section. The initial mesh of the brain slice is a triangular mesh composed of 43 402 elements constructed using VMTK [43]. As presented in [44, §5.1], the final mesh is a polygonal mesh consisting of 534 elements constructed by agglomerating the elements of the initial triangular mesh. The use of a DG method allows for meshes with elements of fairly general shape, while the construction of agglomerated elements helps to reduce the computational cost. Each element is labeled as either white or grey matter, according to

$h \approx 0.4278$ and $\tau = 2.5 \times 10^{-2}$

Method		$\ell = 1$	$\ell = 2$	$\ell = 3$	$\ell = 4$	$\ell = 5$
BDF1	SP-LDG	4.72×10^{-2}	2.28×10^{-2}	1.50×10^{-2}	1.29×10^{-1}	1.43×10^{-2}
	IPDG	1.06	5.98	3.33×10^2	1.43×10^{-2}	1.43×10^{-2}
BDF2	SP-LDG	4.72×10^{-2}	3.73×10^{-3}	1.13×10^{-3}	2.84×10^{-4}	2.50×10^{-4}
	CN IPDG	3.38×10^3	1.90×10^3	2.33×10^1	1.15×10^{-1}	7.68×10^{-3}

$h \approx 0.2309$ and $\tau = 2.5 \times 10^{-2}$

Method		$\ell = 1$	$\ell = 2$	$\ell = 3$	$\ell = 4$	$\ell = 5$
BDF1	SP-LDG	4.67×10^{-2}	1.31×10^{-2}	1.43×10^{-2}	1.43×10^{-2}	1.02×10^{-2}
	IPDG	1.05	1.07	4.32×10^{-2}	1.66×10^{-2}	1.69×10^{-2}
BDF2	SP-LDG	3.18×10^{-2}	1.44×10^{-3}	2.46×10^{-4}	2.52×10^{-4}	2.84×10^{-4}
	CN IPDG	3.13×10^3	9.66×10^4	3.55×10^{-2}	6.17×10^{-4}	9.21×10^{-5}

$h \approx 0.4278$ and $\tau = 5.0 \times 10^{-3}$

Method		$\ell = 1$	$\ell = 2$	$\ell = 3$	$\ell = 4$	$\ell = 5$
BDF1	SP-LDG	3.66×10^{-2}	5.34×10^{-3}	4.91×10^{-3}	4.20×10^{-3}	4.25×10^{-3}
	IPDG	1.37	2.89	2.62×10^3	4.51×10^{-3}	2.97×10^{-3}
BDF2	SP-LDG	3.14×10^{-2}	4.48×10^{-3}	8.59×10^{-4}	1.15×10^{-4}	2.55×10^{-5}
	CN IPDG	2.51×10^4	2.60×10^4	1.59×10^4	4.47×10^{-4}	2.77×10^{-4}

$h \approx 0.2309$ and $\tau = 5.0 \times 10^{-3}$

Method		$\ell = 1$	$\ell = 2$	$\ell = 3$	$\ell = 4$	$\ell = 5$
BDF1	SP-LDG	3.46×10^{-2}	1.97×10^{-3}	2.81×10^{-3}	2.82×10^{-3}	2.83×10^{-3}
	IPDG	1.08	1.09	3.65×10^{-2}	3.05×10^{-3}	3.33×10^{-3}
BDF2	SP-LDG	3.17×10^{-2}	1.62×10^{-3}	1.54×10^{-5}	1.05×10^{-5}	1.03×10^{-5}
	CN IPDG	2.75×10^4	3.39×10^4	3.55×10^{-2}	6.57×10^{-4}	3.97×10^{-5}

Table 2: Computed errors in the $L^2(\Omega)$ norm at final time $T = 10$ with different methods (SP-LDG and IPDG [19]).

the segmentation of magnetic resonance images. Another advantage of mesh agglomeration is that it allows the external boundary and the internal interface between white and grey matter to be described using just a few polygonal elements.

In the simulations, we set the physical parameters as follows [40, 45]: the reaction coefficient is

$$\alpha = \alpha(\mathbf{x}) = \begin{cases} 0.45 \text{ year}^{-1} & \text{in the grey matter,} \\ 0.9 \text{ year}^{-1} & \text{in the white matter,} \end{cases}$$

and the diffusion tensor, which is isotropic in the grey matter and anisotropic in the white matter, is

$$\mathbf{D} = \mathbf{D}(\mathbf{x}) = \begin{cases} d_{\text{ext}} \mathbb{I}_2 & \text{in the grey matter,} \\ d_{\text{ext}} \mathbb{I}_2 + d_{\text{axn}} \mathbf{a}(\mathbf{x}) \otimes \mathbf{a}(\mathbf{x}) & \text{in the white matter,} \end{cases}$$

with isotropic diffusion with the same coefficient $d_{\text{ext}} = 8 \text{ mm}^2/\text{year}$, and additional anisotropic diffusion in the white matter 10 times faster, namely $d_{\text{axn}} = 80 \text{ mm year}^{-1}$. The latter is associated with axonal directions $\mathbf{a} = \mathbf{a}(\mathbf{x})$, with $|\mathbf{a}| = 1$, derived from diffusion-weighted images as in [19]. The diffusion tensor \mathbf{D} is uniformly positive definite in the domain, with constant larger than or equal to d_{ext} .

Concerning the numerical discretization of the problem, we use polynomials of degree $\ell = 2$, the power-mean parameter $\theta = 1/2$ in (2.11), and a stabilization parameter $\eta_0 = 2$ for the space discretization. For the time discretization, we choose a time step $\tau = 2.5 \times 10^{-2}$ year, a final time $T = 25$ years, and we use the BDF6 time-stepping scheme. We set the stabilization parameter $\varepsilon = 10^{-8}$.

We start the simulations of α -synuclein diffusion from two different initial conditions for the misfolded proteins: in the first case, they are located in the dorsal motor nucleus, namely, at the base of the brainstem; in the second one, they are located in the limbic region, just under the ventricles [39].

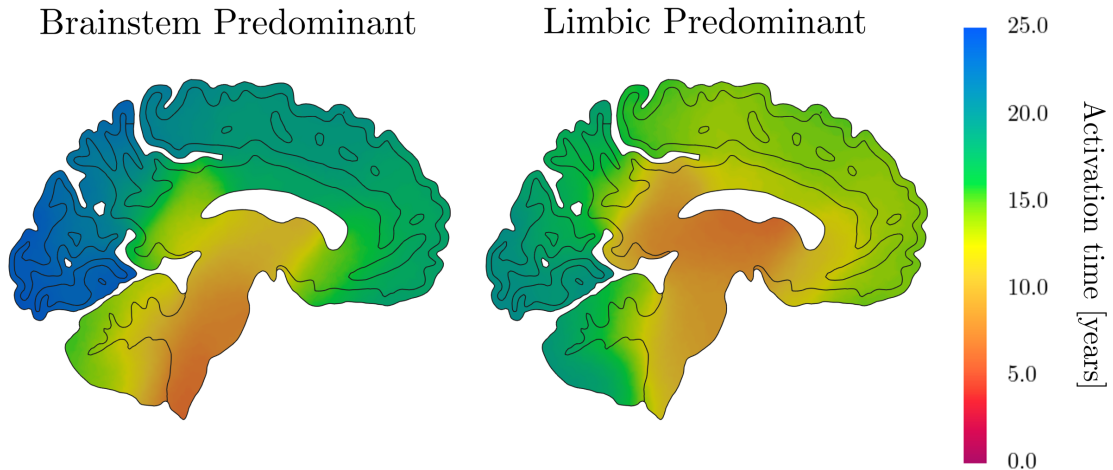


Figure 8: Test case 3: Activation time patterns of α -synuclein propagation for the brainstem (left) and limbic predominant (right) prodromal evolutions of the pathology.

In Figure 7, we report the initial conditions at time $t = 0$ and the computed solutions at different times $t = 5, 10, 15, 20$ years. It can be observed that both starting with a brainstem or a limbic predominant concentration, the next stage of the propagation is associated with the presence of Lewy bodies in both regions, see Figure 7, $t = 10$ years. Finally, the spread of the α -synuclein continues into the neocortical area, as visible in Figure 7 ($t = 15, 20$ years). This pathological progress is coherent with the medical literature findings of USSLB theory [39]. Medical literature describes that a limbic-predominant Lewy body pathology is more associated with early cognitive decline [46]. This is coherent with the earlier involvement of the neocortex resulting from our numerical simulation.

Finally, to quantify the development of the pathology, we compute the activation time as defined in [19]:

$$\hat{t}(\mathbf{x}) = \int_0^T \chi_{\{c_h(\mathbf{x},s) < c_{\text{crit}}\}}(\mathbf{x}, s) ds \quad \mathbf{x} \in \Omega, \quad (4.1)$$

where χ is the indicator function and c_{crit} is the critical value of the pathological protein concentration. This indicator provides a measure of the time at which the concentration of misfolded proteins exceeds a certain threshold, after which we assume the neurons in a specific region could be affected by pathological communication induced by the induced toxicity [47]. In this test case, we fix the threshold to be equal to $c_{\text{crit}} = 0.95$. We report the computed activation time in Figure 8. The pattern of the brainstem predominant activation is consistent with existing literature results obtained using other numerical methods [19, 44]. Comparing the result of the cases with brainstem and limbic predominant phase, we observe that, in the latter case, the neocortex is affected for a shorter duration (12–20 years). In contrast, the average activation time of the neocortex in the brainstem predominant case is about 18–25 years. This confirms the early cognitive decline of the limbic predominant Lewy body pathology [46].

5 Conclusions

This work has introduced a structure-preserving, high-order, unconditionally stable numerical method for approximating the solution to the Fisher-Kolmogorov equation on general polytopal meshes, with a particular focus on modeling the spread of misfolded proteins in neurodegenerative diseases. The proposed approach is based on an entropy-variable reformulation of the model problem to ensure positivity, boundedness, and satisfaction of a discrete entropy-stability inequality at the discrete level. The numerical scheme employs a local discontinuous Galerkin (LDG) method on polytopal meshes for the spatial discretization, coupled with a ν -step backward differentiation formula for the time discretization. We have discussed implementation details, highlighting the derivation and solution of the linear systems arising from Newton’s iterations. The accuracy and robustness of the proposed BDF-LDG method have been demonstrated through a series of numerical experiments. We

have also discussed numerical results obtained for the application of interest, namely, modeling the dynamics of neurodegenerative disorders. In this context, we have presented numerical results showcasing the simulation of α -synuclein propagation in a two-dimensional brain geometry reconstructed from MRI data, thereby offering a promising computational tool for studying synucleopathies, such as Parkinson’s disease and dementia with Lewy bodies. Future developments include the theoretical analysis of the proposed approach, which is currently under investigation. Additionally, extending to three-dimensional testing represents a natural direction for further research. Moreover, integrating data assimilation techniques and uncertainty quantification will be crucial for enhancing the clinical relevance of the proposed computational framework.

Acknowledgements

The first three authors were partially supported by the European Union (ERC Synergy, NEMESIS, project number 101115663). Views and opinions expressed are, however, those of the authors only and do not necessarily reflect those of the EU or the ERC Executive Agency. The first three authors are also members of the INdAM-GNCS group. This research was funded in part by the Austrian Science Fund (FWF) project 10.55776/F65. The present research is part of the activities of Dipartimento di Eccellenza 2023-2027.

The brain MRI images were provided by OASIS-3: Longitudinal Multimodal Neuroimaging: Principal Investigators: T. Benzinger, D. Marcus, J. Morris; NIH P30 AG066444, P50 AG00561, P30 NS09857781, P01 AG026276, P01 AG003991, R01 AG043434, UL1 TR000448, R01 EB009352. AV-45 doses were provided by Avid Radiopharmaceuticals, a wholly-owned subsidiary of Eli Lilly.

References

- [1] R. A. Fisher, “The wave of advance of advantageous genes,” *Ann. Eugenics*, vol. 7, 1937.
- [2] S. Fornari, A. Schäfer, M. Jucker, A. Goriely, and E. Kuhl, “Prion-like spreading of Alzheimer’s disease within the brain’s connectome,” *J. R. Soc. Interface*, vol. 16, no. 159, p. 20190356, 2019.
- [3] T. G. Beach, C. H. Adler, L. Lue, L. I. Sue, J. Bachalakuri, J. Henry-Watson, J. Sasse, S. Boyer, S. Shirohi, R. Brooks, J. Eschbacher, C. L. White, H. Akiyama, J. Caviness, H. A. Shill, D. J. Connor, M. N. Sabbagh, D. G. Walker, and the Arizona Parkinson’s Disease Consortium, “Unified staging system for Lewy body disorders: correlation with nigrostriatal degeneration, cognitive impairment and motor dysfunction,” *Acta Neuropathol.*, vol. 117, no. 6, pp. 613–634, 2009.
- [4] G. S. Bloom, “Amyloid- β and tau: the trigger and bullet in Alzheimer disease pathogenesis,” *JAMA Neurol.*, vol. 71, no. 4, pp. 505–508, 2014.
- [5] S. Salsa and G. Verzini, *Partial differential equations in action. From modelling to theory*, vol. 147 of *Unitext*. Cham: Springer, 4th updated edition ed., 2022.
- [6] P. Lasaint and P.-A. Raviart, “On a finite element method for solving the neutron transport equation,” in *Mathematical aspects of finite elements in partial differential equations (Proc. Sympos., Math. Res. Center, Univ. Wisconsin, Madison, Wis., 1974)*, pp. 89–123, Academic Press, New York-London, 1974.
- [7] J. Nitsche, “Über ein Variationsprinzip zur Lösung von Dirichlet-Problemen bei Verwendung von Teilräumen, die keinen Randbedingungen unterworfen sind,” *Abh. Math. Sem. Univ. Hamburg*, vol. 36, pp. 9–15, 1971.
- [8] G. A. Baker, “Finite element methods for elliptic equations using nonconforming elements,” *Math. Comp.*, vol. 31, no. 137, pp. 45–59, 1977.
- [9] P. Percell and M. F. Wheeler, “A local residual finite element procedure for elliptic equations,” *SIAM J. Numer. Anal.*, vol. 15, no. 4, pp. 705–714, 1978.
- [10] M. F. Wheeler, “An elliptic collocation-finite element method with interior penalties,” *SIAM J. Numer. Anal.*, vol. 15, no. 1, pp. 152–161, 1978.
- [11] D. N. Arnold, “An interior penalty finite element method with discontinuous elements,” *SIAM J. Numer. Anal.*, vol. 19, no. 4, pp. 742–760, 1982.

- [12] D. N. Arnold, F. Brezzi, B. Cockburn, and L. D. Marini, “Unified analysis of discontinuous Galerkin methods for elliptic problems,” *SIAM J. Numer. Anal.*, vol. 39, no. 5, pp. 1749–1779, 2001/02.
- [13] P. F. Antonietti, F. Brezzi, and L. D. Marini, “Bubble stabilization of discontinuous Galerkin methods,” *Comput. Methods Appl. Mech. Engrg.*, vol. 198, no. 21-26, pp. 1651–1659, 2009.
- [14] F. Bassi, L. Botti, A. Colombo, D. A. Di Pietro, and P. Tesini, “On the flexibility of agglomeration based physical space discontinuous Galerkin discretizations,” *J. Comput. Phys.*, vol. 231, no. 1, pp. 45–65, 2012.
- [15] P. F. Antonietti, S. Giani, and P. Houston, “*hp*-version composite discontinuous Galerkin methods for elliptic problems on complicated domains,” *SIAM J. Sci. Comput.*, vol. 35, no. 3, pp. A1417–A1439, 2013.
- [16] A. Cangiani, E. H. Georgoulis, and P. Houston, “*hp*-version discontinuous Galerkin methods on polygonal and polyhedral meshes,” *Math. Models Methods Appl. Sci.*, vol. 24, no. 10, pp. 2009–2041, 2014.
- [17] A. Cangiani, Z. Dong, E. H. Georgoulis, and P. Houston, *hp-version discontinuous Galerkin methods on polygonal and polyhedral meshes*. SpringerBriefs in Mathematics, Springer, Cham, 2017.
- [18] P. F. Antonietti, C. Facciola, P. Houston, I. Mazzieri, G. Pennesi, and M. Verani, “High-order discontinuous Galerkin methods on polyhedral grids for geophysical applications: seismic wave propagation and fractured reservoir simulations,” in *Polyhedral Methods in Geosciences*, pp. 159–225, Cham: Springer, 2021.
- [19] M. Corti, F. Bonizzoni, L. Dede, A. M. Quarteroni, and P. F. Antonietti, “Discontinuous Galerkin methods for Fisher-Kolmogorov equation with application to α -synuclein spreading in Parkinson’s disease,” *Comput. Methods Appl. Mech. Engrg.*, vol. 417, pp. Paper No. 116450, 17, 2023.
- [20] P. F. Antonietti, F. Bonizzoni, M. Corti, and A. Dall’Olio, “Discontinuous Galerkin approximations of the heterodimer model for protein-protein interaction,” *Comput. Methods Appl. Mech. Engrg.*, vol. 431, pp. Paper No. 117282, 17, 2024.
- [21] P. F. Antonietti, M. Corti, and G. Lorenzon, “A discontinuous Galerkin method for the three-dimensional heterodimer model with application to prion-like proteins’ dynamics,” tech. rep., MOX Report 51/2024, 2024. [arXiv:2407.16065](https://arxiv.org/abs/2407.16065).
- [22] L. Guo and Y. Yang, “Positivity preserving high-order local discontinuous Galerkin method for parabolic equations with blow-up solutions,” *J. Comput. Phys.*, vol. 289, pp. 181–195, 2015.
- [23] Z. Sun, J. A. Carrillo, and C.-W. Shu, “A discontinuous Galerkin method for nonlinear parabolic equations and gradient flow problems with interaction potentials,” *J. Comput. Phys.*, vol. 352, pp. 76–104, 2018.
- [24] R. Zhang, J. Zhu, A. F. D. Loula, and X. Yu, “Operator splitting combined with positivity-preserving discontinuous Galerkin method for the chemotaxis model,” *J. Comput. Appl. Math.*, vol. 302, pp. 312–326, 2016.
- [25] J. E. Macías-Díaz and A. Puri, “An explicit positivity-preserving finite-difference scheme for the classical Fisher-Kolmogorov-Petrovsky-Piscounov equation,” *Appl. Math. Comput.*, vol. 218, no. 9, pp. 5829–5837, 2012.
- [26] S. Hasnain, M. Saqib, and D. Suleiman Mashat, “Numerical study of one dimensional Fisher’s KPP equation with finite difference schemes,” *Amer. J. Comput. Math.*, vol. 7, pp. 70–83, 2017.
- [27] O. P. Yadav and R. Jiwari, “Finite element analysis and approximation of Burgers’-Fisher equation,” *Numer. Methods Partial Differential Equations*, vol. 33, no. 5, pp. 1652–1677, 2017.
- [28] F. Bonizzoni, M. Braukhoff, A. Jüngel, and I. Perugia, “A structure-preserving discontinuous Galerkin scheme for the Fisher-KPP equation,” *Numer. Math.*, vol. 146, no. 1, pp. 119–157, 2020.
- [29] S. Gómez, A. Jüngel, and I. Perugia, “Structure-preserving Local Discontinuous Galerkin method for nonlinear cross-diffusion systems.” [arXiv:2406.17900](https://arxiv.org/abs/2406.17900), 2024.
- [30] A. Jüngel, “The boundedness-by-entropy method for cross-diffusion systems,” *Nonlinearity*, vol. 28, no. 6, pp. 1963–2001, 2015.

- [31] Z. Dong and E. H. Georgoulis, “Robust interior penalty discontinuous Galerkin methods,” *J. Sci. Comput.*, vol. 92, no. 2, pp. Paper No. 57, 23, 2022.
- [32] A. Ern, A. F. Stephansen, and P. Zunino, “A discontinuous Galerkin method with weighted averages for advection-diffusion equations with locally small and anisotropic diffusivity,” *IMA J. Numer. Anal.*, vol. 29, no. 2, pp. 235–256, 2009.
- [33] E. Hairer, S. P. Nørsett, and G. Wanner, *Solving ordinary differential equations. I: Nonstiff problems.*, vol. 8 of *Springer Ser. Comput. Math.* Berlin: Springer-Verlag, 2. rev. ed. ed., 1993.
- [34] J. D. Lambert, *Numerical Methods for Ordinary Differential Systems: The Initial Value Problem.* John Wiley & Sons, Ltd., Chichester, 1991.
- [35] P. F. Antonietti, S. Bonetti, M. Botti, M. Corti, I. Fumagalli, and I. Mazzieri, “**lymph**: discontinuous polytopal methods for Multi-PHysics differential problems,” *ACM Trans. Math. Softw.*, vol. 51, no. 1, pp. 3:1–3:22, 2025.
- [36] C. Talischi, G. H. Paulino, A. P., and I. F. M. Menezes, “**PolyMesher**: a general-purpose mesh generator for polygonal elements written in Matlab,” *Struct. Multidiscip. Optim.*, vol. 45, no. 3, pp. 309–328, 2012.
- [37] D. Wen-Shan, Y. Hong-Juan, and S. Yu-Ren, “An exact solution of Fisher equation and its stability,” *Chinese Phys.*, vol. 15, no. 7, p. 1414, 2006.
- [38] T. G. Beach, C. H. Adler, L. I. Sue, L. Vedders, L. Lue, C. L. White III, H. Akiyama, J. N. Caviness, H. A. Shill, M. N. Sabbagh, D. G. Walker, and Arizona Parkinson’s Disease Consortium, “Multi-organ distribution of phosphorylated α -synuclein histopathology in subjects with Lewy body disorders,” *Acta Neuropathol.*, vol. 119, no. 6, pp. 689–702, 2010.
- [39] C. H. Adler, T. G. Beach, N. Zhang, H. A. Shill, E. Driver-Dunckley, J. N. Caviness, S. H. Mehta, M. N. Sabbagh, G. E. Serrano, L. I. Sue, C. M. Belden, J. Powell, S. A. Jacobson, E. Zamrini, D. Shprecher, K. J. Davis, B. N. Dugger, and J. G. Hentz, “Unified staging system for Lewy body disorders: Clinicopathologic correlations and comparison to Braak staging,” *J. Neuropathol. Exp. Neurol.*, vol. 78, no. 10, pp. 891–899, 2019.
- [40] J. Weickenmeier, M. Jucker, A. Goriely, and E. Kuhl, “A physics-based model explains the prion-like features of neurodegeneration in Alzheimer’s disease, Parkinson’s disease, and amyotrophic lateral sclerosis,” *J. Mech. Phys. Solids*, vol. 124, pp. 264–281, 2019.
- [41] T. B. Thompson, P. Chaggar, E. Kuhl, A. Goriely, and ADNI, “Protein-protein interactions in neurodegenerative diseases: A conspiracy theory,” *PLOS Comput. Biol.*, vol. 16, no. 10, p. e1008267, 2020.
- [42] P. J. LaMontagne, T. L. Benzinger, J. C. Morris, S. Keefe, R. Hornbeck, C. Xiong, E. Grant, J. Hassenstab, K. Moulder, A. G. Vlassenko, M. E. Raichle, C. Cruchaga, and D. Marcus, “OASIS-3: Longitudinal neuroimaging, clinical, and cognitive dataset for normal aging and Alzheimer disease.” medRxiv, 2019. <https://doi.org/10.1101/2019.12.13.19014902>.
- [43] L. Antiga, M. Piccinelli, L. Botti, B. Ene-Iordache, A. Remuzzi, and D. A. Steinman, “An image-based modeling framework for patient-specific computational hemodynamics,” *Med. Biol. Eng. Comput.*, vol. 46, no. 11, pp. 1097–1112, 2008.
- [44] M. Corti, F. Bonizzoni, and P. F. Antonietti, “Structure preserving polytopal discontinuous Galerkin methods for the numerical modeling of neurodegenerative diseases,” *J. Sci. Comput.*, vol. 100, no. 2, pp. Paper No. 39, 24, 2024.
- [45] A. Schäfer, J. Weickenmeier, and E. Kuhl, “The interplay of biochemical and biomechanical degeneration in Alzheimer’s disease,” *Comput. Methods Appl. Mech. Engrg.*, vol. 352, pp. 369–388, 2019.
- [46] M. G. Cersosimo, “Propagation of alpha-synuclein pathology from the olfactory bulb: possible role in the pathogenesis of dementia with Lewy bodies,” *Cell Tissue Res.*, vol. 373, no. 1, pp. 233–243, 2018.
- [47] H. Braak, K. Del Tredici, U. Rüb, R. A. de Vos, E. N. Jansen Steur, and E. Braak, “Staging of brain pathology related to sporadic Parkinson’s disease,” *Neurobiol. Aging*, vol. 24, no. 2, pp. 197–211, 2003.